AD-A278 640

AFOSR-TR- 94 0263

Approved for public release;
distribution unlimited.

Final Report

Aeroservoelastic Tailoring with Adaptive Materials

AFOSR Grant 91-0386

Professor Terrence A. Weisshaar
Principal Investigator

Professor Mario Rotea
Faculty Associate

School of Aeronautics and Astronautics
Purdue University
West Lafayette, Indiana 47907-1282

March 3, 1994

DTIC
ELECTE
APR 29 1994
S B D

DISTRIBUTION STATEMENT A
Approved for public release;
Distribution Unlimited

94-12936

94 4 28 042

REPORT DOCUMENTATION PAGE

Form Approved
OMB No. 0704-0188

1. AGENCY USE ONLY (Leave blank)	2. REPORT DATE	3. REPORT TYPE AND DATES COVERED
	9 February 1994	FINAL REPORT - 1 Oct. 1991 - 30 Sept. 1993

4. TITLE AND SUBTITLE
Aeroservoelastic Tailoring with Piezoelectric Materials: Actuator optimization studies

5. FUNDING NUMBERS
G 91-0386 AFOSR

6. AUTHOR(S)
Terrence A. Weisshaar
Mario A. Rotea

7. PERFORMING ORGANIZATION NAME(S) AND ADDRESS(ES)
School of Aeronautics and Astronautics
Purdue University
West Lafayette, IN 47907-1282

8. PERFORMING ORGANIZATION REPORT NUMBER
AERO - 3
AFOSR-TR- 94 0263

9. SPONSORING/MONITORING AGENCY NAME(S) AND ADDRESS(ES)
Air Force Office of Scientific Research
AFOSR/NA
110 Duncan Ave., Suite B115
Bolling AFB, DC 20332-0001

10. SPONSORING/MONITORING AGENCY REPORT NUMBER

11. SUPPLEMENTARY NOTES

12a. DISTRIBUTION/AVAILABILITY STATEMENT
Approved for public release;
distribution unlimited.

12b. DISTRIBUTION CODE

13. ABSTRACT (Maximum 200 words)

This report summarizes aeroservoelastic tailoring studies in which adaptive material actuators are used to control structural deflection of aeroelastic systems. The problem is to furnish enough directed control of a system to make the control of the phenomenon feasible. Specific research problems considered are: choice of the actuator material fro effective control; geometric arrangement for active control; and optimum coverage of surface panels for effective control. A specific method of controller design is suggested to determine the limits of control. It is applied to a typical section whose response to random atmospheric turbulence is to be controlled. A finite element method is developed to model actuator and sensor output for plate-like actuators and its use is illustrated for wing-like configurations to demonstrate the benefits of orthotropic material actuators. Finally, the problem of optimum actuators to supply deflection of panels for wing surfaces is examined to determine optimality criteria for such panels and to use strain energy as a guide for efficient use of actuator/host plate combinations.

14. SUBJECT TERMS
Piezoelectric actuators, aeroservoelasticity

DTIC QUALITY INSPECTED 3

15. NUMBER OF PAGES
42

16. PRICE CODE

17. SECURITY CLASSIFICATION OF REPORT	18. SECURITY CLASSIFICATION OF THIS PAGE	19. SECURITY CLASSIFICATION OF ABSTRACT	20. LIMITATION OF ABSTRACT
UNCLASSIFIED	UNCLASSIFIED	UNCLASSIFIED	UL

NSN 7540-01-280-5500

Standard Form 298 (Rev. 2-89)
Prescribed by ANSI Std. Z39-18

GENERAL INSTRUCTIONS FOR COMPLETING SF 298

The Report Documentation Page (RDP) is used in announcing and cataloging reports. It is important that this information be consistent with the rest of the report, particularly the cover and title page. Instructions for filling in each block of the form follow. It is important to stay within the lines to meet *optical scanning requirements*.

Block 1. Agency Use Only (Leave blank).

Block 2. Report Date. Full publication date including day, month, and year, if available (e.g. 1 Jan 88). Must cite at least the year.

Block 3. Type of Report and Dates Covered. State whether report is interim, final, etc. If applicable, enter inclusive report dates (e.g. 10 Jun 87 - 30 Jun 88).

Block 4. Title and Subtitle. A title is taken from the part of the report that provides the most meaningful and complete information. When a report is prepared in more than one volume, repeat the primary title, add volume number, and include subtitle for the specific volume. On classified documents enter the title classification in parentheses.

Block 5. Funding Numbers. To include contract and grant numbers; may include program element number(s), project number(s), task number(s), and work unit number(s). Use the following labels:

C	- Contract	PR	- Project
G	- Grant	TA	- Task
PE	- Program Element	WU	- Work Unit Accession No.

Block 6. Author(s). Name(s) of person(s) responsible for writing the report, performing the research, or credited with the content of the report. If editor or compiler, this should follow the name(s).

Block 7. Performing Organization Name(s) and Address(es). Self-explanatory.

Block 8. Performing Organization Report Number. Enter the unique alphanumeric report number(s) assigned by the organization performing the report.

Block 9. Sponsoring/Monitoring Agency Name(s) and Address(es). Self-explanatory.

Block 10. Sponsoring/Monitoring Agency Report Number. *(If known)*

Block 11. Supplementary Notes. Enter information not included elsewhere such as: Prepared in cooperation with...; Trans. of...; To be published in.... When a report is revised, include a statement whether the new report supersedes or supplements the older report.

Block 12a. Distribution/Availability Statement. Denotes public availability or limitations. Cite any availability to the public. Enter additional limitations or special markings in all capitals (e.g. NOFORN, REL, ITAR).

- DOD - See DoDD 5230.24, "Distribution Statements on Technical Documents."
- DOE - See authorities.
- NASA - See Handbook NHB 2200.2.
- NTIS - Leave blank.

Block 12b. Distribution Code.

- DOD - Leave blank.
- DOE - Enter DOE distribution categories from the Standard Distribution for Unclassified Scientific and Technical Reports.
- NASA - Leave blank.
- NTIS - Leave blank.

Block 13. Abstract. Include a brief *(Maximum 200 words)* factual summary of the most significant information contained in the report.

Block 14. Subject Terms. Keywords or phrases identifying major subjects in the report.

Block 15. Number of Pages. Enter the total number of pages.

Block 16. Price Code. Enter appropriate price code *(NTIS only)*.

Blocks 17. - 19. Security Classifications. Self-explanatory. Enter U.S. Security Classification in accordance with U.S. Security Regulations (i.e., UNCLASSIFIED). If form contains classified information, stamp classification on the top and bottom of the page.

Block 20. Limitation of Abstract. This block must be completed to assign a limitation to the abstract. Enter either UL (unlimited) or SAR (same as report). An entry in this block is necessary if the abstract is to be limited. If blank, the abstract is assumed to be unlimited.

Final Report

Aeroservoelastic Tailoring with Adaptive Materials

AFOSR Grant 91-0386

Professor Terrence A. Weisshaar
Principal Investigator

Professor Mario Rotea
Faculty Associate

School of Aeronautics and Astronautics
Purdue University
West Lafayette, Indiana 47907-1282

March 3, 1994

Abstract

This report summarizes aeroservoelastic tailoring studies in which adaptive material actuators are used to control structural deflection of aeroelastic systems. The actuator must furnish enough control of a system to make the control of the phenomenon feasible. Specific research problems considered are: choice of the actuator material for effective control; geometric arrangement of actuators for active control; and optimum coverage of surface panels for effective control; a controller design process to improve efficiency of the selection process. A finite element method is developed to model actuator and sensor output for plate-like actuators and its use is illustrated for wing-like configurations to demonstrate the benefits of orthotropic material actuators. The problem of optimum actuators to supply deflection of panels for wing surfaces is examined to determine optimality criteria for such panels and to use strain energy as a guide for efficient use of actuator/host plate combinations. Finally, a method of controller design is suggested to determine the limits of actuator control effectiveness for a typical section whose response to random atmospheric turbulence is to be minimized.

Accession For
NTIS GRA&I ☑
DTIC TAB ☐
Unannounced ☐
Justification
By
Distribution/
Availability Codes
Dist | Avail and/or Special
A-1

Table of Contents

Section	Title	Page
1.0	Introduction	1
1.1	Purpose and Scope	1
1.2	Summary of Research Efforts - Publications and Education	1
1.3	Controlled structure synthesis	2
1.4	Issues with integrated active material sensor/actuators for aeroservoelasticity	3
2.0	Actuator optimization and analysis	5
2.1	Purpose and scope - aeroelastic load control	5
2.2	Summary of finite element development and studies	6
2.3	Panel actuator combinations for maximum deflection - optimality criteria	7
2.4	Summary	8
3.0	Active control of a typical section	8
	References	19
	Appendix	20
Technical papers		21

"Active Tailoring of adaptive lifting surfaces for aeroelastic applications"
M.N. Abdul-Wahed and T.A. Weisshaar, presented at the
1993 North American Conference on Smart Structures and Materials,
Albuquerque, N.M., Feb. 1993

"Optimizing induced strain actuators for maximum panel deflection"
T.J. Leeks and T.A. Weisshaar, presented at the
AIAA Adaptive Structures Forum,
Hilton Head, S.C., April 1994.

LIST OF SYMBOLS

b	=	airfoil semi-chord dimension, $b = c/2$
c	=	airfoil chord dimension
e	=	offset distance between airfoil aerodynamic center and shear center, positive aft.
$\bar{e}$	=	$= e/b$
g	=	actuator material active stiffness, as a fraction of airfoil torsional stiffness K_T
h	=	airfoil plunge displacement, measured at the shear center
$\bar{h}$	=	h/b
k	=	actuator material active stiffness, as a fraction of airfoil bending stiffness, K_h
L	=	characteristic length of gust disturbance
m	=	mass of airfoil
U	=	airspeed
$\bar{U}$	=	$U/\omega_\alpha b$
w_g	=	vertical component of gust velocity, feet per second.
α	=	airfoil angle of attack
β	=	aileron rotation angle with respect to parent airfoil
ρ	=	air density
μ	=	nondimensional mass ratio, $\mu = m/\pi\rho b^2$
ω_α	=	uncoupled airfoil torsion frequency
ω_h	=	uncoupled airfoil plunge frequency
$C_{L\alpha}$	=	lift-curve slope for airfoil
$C_{L\beta}$	=	lift-curve slope for aileron
$\frac{\partial\alpha}{\partial\beta}$	=	$\frac{C_{L\beta}}{C_{L\alpha}}$
$C_{M\beta}$	=	pitching moment coefficient at airfoil aerodynamic center due to β
$(\ )'$	=	transpose of vector or matrix
$E\{x(t)\}$	=	mean or expected value of a stationary random process $\{x(t); -\infty < t < \infty\}$
$E\{x^2(t)\}$	=	variance of a zero mean stationary random process $\{x(t); -\infty < t < \infty\}$
$E_\infty\{x(t)\}$	=	$\lim_{t\to\infty} E\{x(t)\}$ steady-state mean of an asymptotically stationary random process $\{x(t); t \geq 0\}$
$E_\infty\{x^2(t)\}$	=	$\lim_{t\to\infty} E\{x^2(t)\}$ steady-state variance of a zero mean asymptotically stationary random process $\{x(t); t \geq 0\}$

Section 1.0 - Introduction

1.1 Purpose and Scope

This report summarizes studies conducted between 1 October 1991 and 30 September 1993. The purpose of this research was to develop fundamental understanding of the features of successful integrated aeroservoelastic design when active materials are used as actuators to control the deformation of lifting surfaces. Key features of this study focus on the development of appropriate models and identification of effective analytical techniques.

The first problem studied is the process of actuator material selection and development new a finite element model and optimization studies to determine the conditions for optimality of actuator host plate configurations. This latter effort led to a strain energy approach for actuator design. Secondly, the research examined the conditions for the effective integration of control estimation theory into the aeroelastic process when active materials were used. This effort produced results summarized in Section 3.0.

1.2 Summary of Research Efforts - Publications and Education

As the result of this research funding, one Master's Degree student, Ms. Tamara Leeks, was funded for her early research work, as a student of the Principal Investigator, Professor Weisshaar. She later received a National Science Foundation Fellowship to continue her studies into the Ph.D. program. Ms. Leeks received her M.S. degree in December 1993 and is now a Ph.D. student at Purdue, continuing her research on piezoelectric actuators. Ms. Leeks and Professor Weisshaar will present a paper at an AIAA Conference in April 1993 based on results obtained under this AFOSR grant sponsorship.

Professor Mario Rotea, Faculty Associate, also furthered his research efforts in the design of effective controllers for active aeroelastic control. He is the author of the work covered in Section 3. He is now a National Science Foundation Presidential Young Investigator.

This funding also supported Professor Weisshaar's efforts to develop advanced finite element analysis models by allowing leveraging funding for collaboration with a Fulbright visiting scholar, Professor M.N. Abdul-Wahed. The results of this collaboration are contained in the Appendix as a paper presented at a national conference.

1.3 Controlled structure synthesis

Lifting surfaces such as wings and stabilizer surfaces are flexible and subject to dynamic response phenomena including flutter, divergence, gust response and buffeting. Because of this, hydraulically driven aerodynamic control surfaces such as ailerons, are used to generate aerodynamic loads. These controlled loads respond to the sensed motion of the parent surface to cancel out objectionable response such as high stresses or structural instabilities.

Lifting surface response in flight is complicated by complex interactions between the flow field around the wing and the response of the wing itself. This interaction is called aeroelasticity. The use of servo controllers to control aeroelastic response is called aeroservoelasticity. Two types of aeroservoelasticity problems were addressed in this study. The first problem is the efficiency of piezoelectric actuators to create and shape the lifting surface loads and structural response. These actuators are imbedded into the structural surface so that they generate load and carry stresses. The second problem development is the modeling of the host structure and its actuators so that effective designs can be evaluated.

The goal of adding an active control system to a structure is to improve performance of the original system by the addition of sensors, control processors and actuators. An even more important goal is to achieve performance that cannot be done in any other practical way. For instance, there may be no uncontrolled structure with the requirements placed on it that fulfills the design goals. A central issue in the design of a controlled structure is the selection and placement of actuators and sensors on and within the system to be controlled.

A well-designed controlled structure is tolerant of imperfections in the system. This feature is called robustness. The controlled system should also have good performance in rejecting system disturbances (gusts for instance). This means that it should attenuate the effects of these disturbances. In the controls community this attenuation is called regulation.

When designing a control system, care must be taken to use a technique that monitors the signals sent by the controller computer to the actuator so that they are not too large so that the actuator limits are exceeded. In the case of an aileron controller, this means that the angle of aileron rotation should not be too large. In the case of a piezoelectric device, it means that the electric field applied to the active material should not be too large.

One major problem with control law evaluation and relating control law requirements to actuator choices is that structural control research has been restricted to a control law

that receives signals from the sensors and changes them into signals to the actuators that are in a specific form. Restricting the form of a control law or confining the study to only one type of solution algorithm is undesirable for two reasons. First of all, when the designer is done, he has not answered the central question that the structural engineer is interested in. This question is :" Have I designed the best possible combination of structure and actuator (including size and location on the structure) so that the result does the job efficiently?" Secondly, when the process is complete it is not certain that the controlled structure represents the best combination of host structure and sensor actuator design.

The method examined in this study was not restricted to a single method of control law design. In fact it will reveal only what the best configuration is, but not the necessary control law. Said differently, this new method will tell us what the limits of performance are, but not how to formulate the control law to get there. This is a key feature of this method. This type of information is more valuable to the structural engineer who is not concerned with the control law algorithm or its development.

1.4 Issues with integrated active material sensor/actuators for aeroservoelasticity

Adaptive structures use actuators to create changes in structural design shape or damping to respond to changing mission needs and performance requirements. Actuators may be articulated mechanical devices such as ailerons and flaps or they may be "smart" materials embedded in the structure. In the case of atmospheric flight vehicles, active material actuators embedded in the structure can control structural shape and aerodynamic loads.

Using sensors and feedback control algorithms, these actuators also can change wing stiffness and control the stability of an entire lifting surface to maneuver and trim an aircraft, reduce gust loads or enhance the stability of the structure. In some cases, this can be done with less weight and at reduced overall cost compared to conventional structures. At present, these concepts rely on aeroelasticity, that is, the mutual interaction between aerodynamic loads and structural deflections, to create favorable active load control.

The design of controlled structures involves trade-offs such as structural stiffnesses, actuator choices and the location of actuators. In aeroservoelastic design, this selection process determines the trade-offs between conventional control surfaces and active materials. Which is more effective in achieving the design goals, the active material or the aerodynamic surface?

Aerodynamic loads, and the local pressures that create these loads, depend on the surface shape on which they act. Surface panels may be flat or curved and are designed to provide aerodynamic shape and to guarantee structural integrity. Re-shaping smooth aero/structural surfaces to change the pressure distribution is done by bonding or otherwise attaching thin actuators to the inside surfaces of structural panels to create an asymmetric configuration that will bend on command.

Thin plate-like or lattice reinforced panels with embedded self-straining actuators such as shape memory materials or piezoelectric materials have been proposed for aerodynamic control concepts that include actively controlled panels to reduce transonic drag and active panel elements to increase supersonic panel flutter speed. For transonic drag reduction, the deformation of a panel on the upper surface of a supercritical airfoil can change the flow field and shock wave intensity to reduce drag on command.

Panel flutter suppression with piezoelectric actuators and shape memory alloy actuators is unique in that no articulated device exists to do the same task. In supersonic flow, dynamic oscillations can be reduced by placing thin actuators on the panel surfaces to change the frequencies of the panels on command.

One problem with active panel concepts is the difficulty finding a design combination to give large enough panel out-of-plane deformations to create the required changes in aerodynamic forces. Without deflections of the order of a panel thickness (or even more), controlling the size and position of the aerodynamic forces is marginal.

A desirable actuator, such as one using today's piezoelectric materials, can not create significant bending deformation of panels unless the host panel/actuator combination is tailored to extract every bit of electro-mechanical efficiency out of the configuration. An emphasis on efficiency naturally leads to considerations of formal optimization that includes a design objective and design variables. However, before formal optimization can proceed, we must select our design variables and determine the sensitivity of the design objective to these design variables.

Section 2 of this report reviews pre-optimization studies to explore the interaction between actuator self-straining ability and bending stiffness, thickness and planform coverage and the host panel bending stiffness and aspect ratio. The purpose of the actuator is to produce large bending deflection. The intent of the study is to identify effective panel/actuator combinations and understand why some combinations are more effective than others.

Section 2.0 - Actuator optimization and analysis studies

2.1 Purpose and scope - aeroelastic load control

This section reviews the purpose and results of to studies related to actuator/host structural matching and optimization for performance of the actuator. Control of aerodynamic loads and structural response of wings and other lifting surfaces is not a new concept. Proposals to control wing response, in particular gust response are over thirty years old. Ride quality enhancement was used on the B-70 Valkerie Supersonic Bomber. The same concept is used today on the B-1 bomber. to allow it to conduct low level , high speed penetration missions. The Lockheed L-1011 uses active inboard flaps to reduce the severity of turbulence on wing fatigue life and on the ride quality felt by passengers.

Suppression of wing flutter, a dynamic structural instability created by unfavorable interaction between unsteady aerodynamic loads and structural vibrations, was demonstrated in the mid-1970's. This flutter suppression was possible by using feedback control to drive aerodynamic surfaces such as ailerons and leading edge slats to damp out motion.

A piezoelectric material is a material which, when subjected to mechanical load, develops an electric charge proportional to the resulting mechanical stress. Conversely, this material will deform or strain when an electric field is applied. This deformation, in particular positive or negative strain, depends on the polarity of the applied field. The electric field is generated by imposing a voltage across the material so that the field is proportional to the applied voltage divided by the distance between the electrodes.

Active materials, in particular piezoelectric material actuators, have been proposed as controllers to accomplish much the same mission as aerodynamic surfaces. How successful and in what areas these material actuators will be able to replace or augment aerodynamic controllers such as ailerons is still very much in doubt. There are advantages to creating so-called "solid state wings" that have no external hinges or mechanical devices. For military applications there is the advantage of stealth. Any gaps or openings that appear in the wing tends to increase size of the radar return from an aircraft. Another advantage is that the control is distributed over the entire wing, making control of some aeroelastic phenomena more precise. Lastly, there are some aeroelastic phenomena, such as panel flutter, for which no mechanical device is feasible.

2.2 Summary of finite element development and studies

The use of actuators to control aeroelastic deformation also depends on their ability to decouple two characteristic types of deformation, bending and twist. This modal decoupling is very important to aeroelastic load control because both types of deformation create aerodynamic loads, but we may not always want these loads to occur simultaneously.

The study of aeroelastic decoupling requires an accurate analytical model, one that can model arrays of anisotropic actuators oriented at angles skewed with respect to conventional structural axes. It also requires realistic modeling of an aircraft wing structure. This model may be a plate-like configuration or the closed box-beam arrangement common to all efficient aeronautical structures.

Because of the interest in effective actuator combinations and realistic structures, a finite element method was developed to model potential structure/actuator configurations. The finite element model consists of three-dimensional isoparametric solid elements (bricks) that allow modeling of tailored piezoelectrics with skewed actuator/sensor axes. This scheme also allows the representation of an anisotropic host structure and can account for material and stacking geometry through the element thickness. Using this finite element representation, it is shown that anisotropic piezoelectric actuators can create sufficient twisting and bending to control aerodynamic loads on a wing.

To illustrate the application of the finite element model developed in the course of this research, this method was used to examine four different actuator/host plate combinations to illustrate orthotropic actuator control and structural response. In one case the deflection of a bimorph plate constructed of two PVDF layers so that the top layer acts as a distributed actuator while the bottom layer acts as a sensor was examined. In another case, a rectangular aluminum plate was sandwiched between two piezoceramic layers and its deflection analyzed to see if bending and torsional deflection could be separated. A similar case considered the same aluminum plate, but with two layers of tailored piezopolymers to assess the effects of piezoelectric anisotropy. Finally, a steel plate was sandwiched between two PVDF elements with off-axis, mirror symmetry to test the ability of a thick layer piezoelectric actuator to deform the plate.

The result of these studies was a paper presented at the North American Conference on Smart Materials and Structures, held in Albuquerque, N.M. in February 1993. This paper is included in the appendix to this report. This paper concluded that:

- Electromechanical anisotropy is an effective and highly desirable, if not essential, to aeroelastic control. Efforts should be directed towards developing more effective

anisotropic materials with larger (and unequal) strain or stress constants (d_{31} or e_{32}) and a larger modulus of elasticity.

- The finite element method can provide an accurate solution for thin and thin-walled structures microactuated by thin piezoelectric elements. This method can readily account for the presence of webs and stiffeners, either active or passive, to study new configurations.

Future work will concentrate on using this finite element model to assess aeroelastic effects on thin plates in supersonic flow and built-up wings in transonic flow. Such configurations can be used to suppress flutter, control shock wave formation and to reduce drag. In addition, this finite element formulation can be used for optimization studies to determine effective actuator geometry and locations and to help to understand issues related to integrating these actuators with host structures.

2.3 Panel actuator combinations for maximum deflection - optimality criteria

Another study conducted with this funding examined the features of a self-straining actuator mounted on one side of a flat panel to cause the largest deflection. A Rayleigh-Ritz model was developed to compute inplane and bending deflections of a plate with an actuator covering only part of the area.

It was shown that it is important to include the coupling terms and the in-plane actuator forces to accurately model the problem. A Rayleigh-Ritz trigonometric series model was developed to analyze the problem and to solve for deflections and stresses. This model allows the actuator to be placed at any location on the panel. It was found that the method gave us excellent results, very close to NASTRAN finite element analysis.

For aluminum panels with aspect ratios between 1.0 and 1.5, the best actuator has a thickness ratio of 0.6 and covers 65% of the panel area. For a panel with an aspect ratio of 3.0, the best actuator has a thickness ratio of 0.6 and covers 70% of the area. For the panels with aspect ratios of 1.0 and 1.5, the actuator with the same aspect ratio as the panel produced the largest deflection. For the panel of aspect ratio 3.0, an actuator with an aspect ratio slightly smaller than that of the panel produced the most deflection.

For a plate with cylindrical bending, when the strain energy is plotted against thickness ratio, an inflection point occurs at the point where the actuator thickness creates the most center panel bending deflection. When the panel is simply supported all around, the plot of strain energy vs. actuator thickness ratio becomes nearly linear at the point

corresponding to the most effective actuator thickness. This indicated that increasing the thickness of the actuator was beneficial until the slope of the strain energy curve reached its smallest value. Adding more thickness to the actuator beyond this point increases stiffness more than it increased the applied moments, and does not increase the deflection that is obtained in the panel.

More precise results for the actuator characteristics could be calculated if an optimization scheme were used in conjunction with the model already developed. Since only a finite number of combinations were tried in this study, the best actuator was found within the limits of the study. Also, the optimal actuator could be found by taking into consideration the weight that is added for a larger actuator. A larger, thicker actuator does not always produce significantly more deflection than a smaller, lighter actuator.

This study was also limited to rectangular actuators placed at any location on the panel. Actuators of shapes other than rectangular should also be considered. Rectangular actuators produce high stresses at the edges and corners. The corner stresses might be avoided if the actuator shape were changed. The deflection produced by elliptical actuators or other actuator shapes should be examined.

2.4 Summary

The analysis necessary to confidently produce optimized actuators for aerodynamic and aeroelastic control has been improved because to the results of the studies just reviewed. Technical papers that detail this research are contained in the Appendix to this report. This research area will also be expanded to be the topic of Ms. Leeks Ph.D. research.

3.0 - Active control of a typical section

This following section summarizes the analysis and methodology developed to use to evaluate the effectiveness of aeroelastic adaptive material actuators. The example chosen is the typical section. The so-called typical section, as originally developed, represented an airfoil section on an unswept wing whose dynamic behavior was typical of the response of the entire wing. This wing section is shown in Figure 2 on the next page.

The essential structural features of this wing model are its two uncoupled natural frequencies, one a torsion reference frequency, ω_α - the other a bending or plunge reference frequency, ω_h. These frequencies are due to elastic restraint provided by the idealized springs depicted in Figure 2. An airstream impinges on the airfoil and generates lift by vortex action. The amount of lift is proportional to the incidence or angle of attack of the surface. This lift is regarded as being generated instantaneously, with no delays or lags between the aerodynamic forces and the displacements.

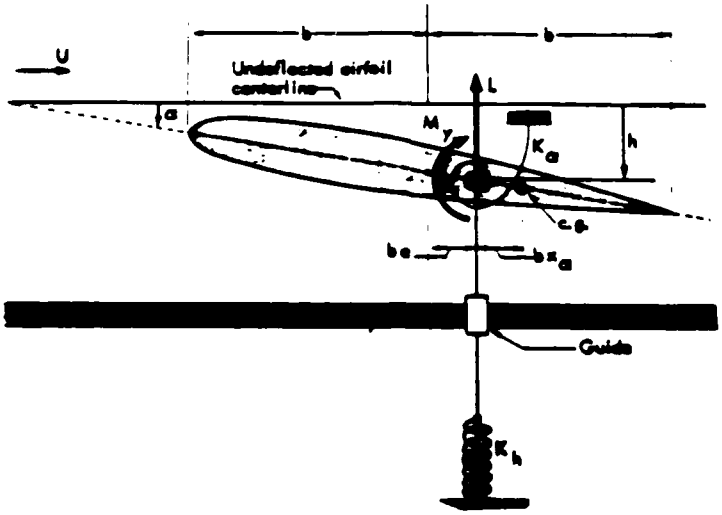

Figure 2: Two-dimensional aeroservoelastic model [2].

The airfoil mass, its moment of inertia and its position relative to the so-called shear center of the section determine the values of the actual airfoil natural frequencies, which are close to ω_α and ω_h when the airstream is not present. These frequencies result from dynamic coupling between the two uncoupled section frequencies. The aerodynamic force and moment are referenced to a point of action called the aerodynamic center, located at the 1/4 chord aft of the leading edge, as shown in Figure 2.

Active control of this section is furnished by some combination of three independent actuators. The first of these controls is the conventional aileron indicated in Figure 2. This aileron has limited effectiveness because it will cause the airfoil to stall and lose lift if it rotates too far with respect to the airfoil. This rotation is represented as β in Figure 2 and its limit is β_o.

The second type of control comes from an adaptive piezoelectric material that applies an internal force to the airfoil at the shear center and also creates an active torsional moment proportional to torsional displacement. This control is furnished by adaptive material

actuators imbedded in the cover skins and the spars of the wing.

The equations of motion for the airfoil section are written in nondimensional form as follows:

$$\mathbf{M}\begin{Bmatrix} \ddot{\bar{h}}(t) \\ \ddot{\alpha}(t) \end{Bmatrix} + (\mathbf{K}_1 + \bar{U}^2\mathbf{K}_2)\begin{Bmatrix} \bar{h}(t) \\ \alpha(t) \end{Bmatrix} = \frac{\bar{U}}{b}\mathbf{F}_g w_g(t) + \mathbf{F}_s\begin{Bmatrix} k(t) \\ g(t) \end{Bmatrix} + \bar{U}^2\mathbf{F}_\beta\beta(t), \quad (1)$$

where

$$\mathbf{M} = \begin{bmatrix} 1 & \bar{x}_\alpha \\ \bar{x}_\alpha & \bar{r}_\alpha^2 \end{bmatrix}, \quad \mathbf{K}_1 = \begin{bmatrix} \omega_h^2 & 0 \\ 0 & \bar{r}_\alpha^2\omega_\alpha^2 \end{bmatrix}, \quad \mathbf{K}_2 = \frac{C_{L_\alpha}}{\mu\pi}\begin{bmatrix} 0 & 1 \\ 0 & -\bar{e} \end{bmatrix},$$

and

$$\mathbf{F}_g = \frac{C_{L_\alpha}}{\mu\pi}\begin{Bmatrix} -\frac{\partial a}{\partial \beta} \\ \bar{e} \end{Bmatrix}, \quad \mathbf{F}_s = \mathbf{K}_1, \quad \mathbf{F}_\beta = \frac{C_{L_\alpha}}{\mu\pi}\begin{Bmatrix} -\frac{\partial a}{\partial \beta} \\ \frac{\partial a}{\partial \beta}\bar{e} + 2\frac{C_{M_\beta}}{C_{L_\alpha}} \end{Bmatrix}.$$

Equation 1 includes the aileron controller, the inertia matrix $\mathbf{M}$ and the stiffness matrix $\mathbf{K}_1$, as discussed previously. It also includes the matrix $\mathbf{K}_2$ that accounts for aerodynamic forces that are functions of airspeed U the displacements, $h(t)$ and $\alpha(t)$. The plunge displacement is divided by the semi-chord dimension $b = c/2$ to obtain the nondimensional signal $\bar{h}(t) = h(t)/b$. Equation 1 contains aerodynamic section coefficients appropriate to the wing.

Flow unsteadiness, an essential feature of models for future study, can be added by modifying the $\mathbf{K}_2$ matrix to include additional degrees of freedom or lag states. However, inclusion of such terms now will unnecessarily complicate the problem.

The presence of adaptive materials is found in the terms k and g in Eqn. 1. These terms are found on the right hand side of that equation. The signal $k(t)$ models the ability of active materials to control the bending stiffness of the section. This signal is bounded and may not exceed the value k_o because of material limitations. Similarly, the signal $g(t)$ models the ability of the active materials to control the torsional stiffness of the wing. This signal can be either independent of $k(t)$ or related to $k(t)$. Here, we assume that $g(t)$ does not depend on $k(t)$ and that $g(t)$ is also bounded and cannot exceed the value g_o. Both k_o and g_o are functions of actuator placement, material properties and geometry.

The equation of motion also contains the influence of a random gust field. This influence is represented by the term w_g, representing the usual Dryden gust field used in aeroelastic design. The signal $w_g(t)$ is the vertical velocity of the gust and is generated by the following

second order dynamical system:

$$\begin{Bmatrix} \dot{\psi}_1(t) \\ \dot{\psi}_2(t) \end{Bmatrix} = \begin{bmatrix} 0 & 1/\tau \\ -1/\tau & -2/\tau \end{bmatrix} \begin{Bmatrix} \psi_1(t) \\ \psi_2(t) \end{Bmatrix} + \begin{bmatrix} 0 \\ 1/\sqrt{\tau} \end{bmatrix} n(t)$$
$$w_g(t) = \psi_1(t) + \sqrt{3}\psi_2(t), \tag{2}$$

where $n(t)$ denotes a stationary white noise signal that excites the gust model, while $\psi_1(t)$ and $\psi_2(t)$ denote the gust states. We assume that $n(t)$ has zero mean and unit r.m.s. value. That is, for all times t, we have $E\{n(t)\} = 0$ and $E\{n^2(t)\} = 1$. Here, $E\{\cdot\}$ denotes the expectation operator. The time constant τ determines the dynamics of the gust model and is given by $\tau = L/U$, where L is the scale length and U the airspeed. The model in Eqn. 2 is scaled so that the steady-state r.m.s. value of $w_g(t)$ is constant and independent of L. This means that $E_\infty\{w_g^2(t)\} = E\{n^2(t)\} = 1$, where $E_\infty\{w_g^2(t)\} = \lim_{t\to\infty} E\{w_g^2(t)\}$ is the steady-state variance of $w_g(t)$.

The three control parameters k, g and β are variables representing the actuator signals available for controlling the structure. The control input is given by the vector

$$\mathbf{u}(t) = \begin{Bmatrix} k(t) \\ g(t) \\ \beta(t) \end{Bmatrix} \tag{3}$$

The controls respond to measured performance of the airfoil. Let $\mathbf{y}$ denote a vector of measurements, corresponding to all positions and velocities available for feedback. This vector is:

$$\mathbf{y}(t) = \begin{Bmatrix} \bar{h}(t) \\ \alpha(t) \\ \dot{\bar{h}}(t) \\ \dot{\alpha}(t) \end{Bmatrix} + \mathbf{v}(t), \tag{4}$$

where $\mathbf{v}(t)$ represents the measurement noise vector. We assume that the measurement noise vector is stationary white noise with zero mean and covariance $E\{\mathbf{v}(t)\mathbf{v}(t)'\} = VI$, where I denotes the identity matrix. The scalar V is the noise intensity. It is also assumed that the measurement noise and the gust excitation are not correlated. It should be noted that this information pattern is not state-feedback in the usual sense because the gust states are not directly available to the controller.

The airfoil dynamics and the gust model are described by a simple block diagram shown in Figure 3. In this diagram the plant $\mathcal{G}$ is the combination of the structure to be controlled

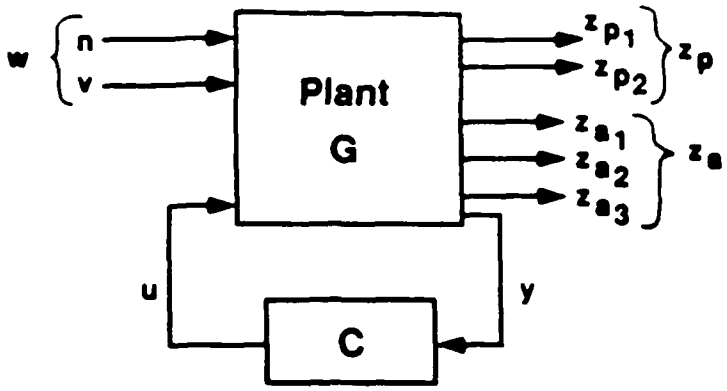

Figure 3: Block diagram of wing section model.

and the gust model, while C denotes an output feedback controller. The controlled signals are composed of performance variables and scaled actuator variables. The performance variables are the plunge and the pitch displacements, and they are defined as:

$$z_{p1}(t) = \frac{\bar{h}(t)}{h_o}, \quad z_{p2}(t) = \frac{\alpha(t)}{\alpha_o} \tag{5}$$

The weighting factors h_o, α_o, are either the nominal values or the maximum values of the corresponding variable. The purpose of these weighting factors is to scale the variables of interest so that they can be compared sensibly. The scaled actuator variables are

$$z_{a1}(t) = \frac{k(t)}{k_o}, \quad z_{a2}(t) = \frac{g(t)}{g_o} \quad z_{a3}(t) = \frac{\beta(t)}{\beta_o} \tag{6}$$

where the scales, or weighting factors, k_o, g_o and β_o are the maximum values or the nominal values of the corresponding actuator variable.

Active control of this model has two objectives, gust alleviation and increasing the flutter speed. For the gust alleviation problem we want to keep the performance signals $z_{p1}(t)$ and $z_{p2}(t)$ ($\bar{h}(t)$ and $\alpha(t)$) "small" despite the presence of the exogenous input $w(t)$ (i.e. the white noise $n(t)$ driving the gust model and the measurement noise $\mathbf{v}(t)$) while also keeping the scaled actuator variables $z_{a1}(t)$, $z_{a2}(t)$, and $z_{a3}(t)$ ($k(t)$, $g(t)$ and $\beta(t)$) within reasonable bounds. We also want to use the active control to increase the flutter speed by at least 10%.

To quantify the above design goals, we need to define mathematically what we mean by a "small" signal. Let C represent a linear time invariant controller that stabilizes the airfoil. When the gust defined in Eqn. 2 enters the closed loop system, and given any initial condition, all the variables in the system approach stationary stochastic processes with zero mean and r.m.s. values that depend on the closed loop system (i.e. they depend on the airfoil structure and the controller). Thus, the ability and effectiveness of the closed loop system to

reject the stochastic gust disturbance and the sensor noise may be determined by measuring the steady state r.m.s. values of the weighted plunge and weighted pitch displacements. Similarly, the activity of each actuator signal can be measured by the steady state r.m.s. value of the corresponding weighted signal.

Mathematically, given a plant $\mathcal{G}$ and a controller $\mathcal{C}$, the performance of the controlled structure is represented by the quantities $E_\infty\{z_{pi}^2(t)\}$, while the actuator activity is given by $E_\infty\{z_{aj}^2(t)\}$. Good disturbance rejection (or good performance) means small r.m.s. values for $z_{p1}(t)$ and $z_{p2}(t)$. Thus, the worst case performance measure for the displacement variables is defined by the function:

$$\phi_{wp}(\mathcal{G},\mathcal{C}) = \max(E_\infty\{z_{p1}^2(t)\}, E_\infty\{z_{p2}^2(t)\}). \tag{7}$$

The function ϕ_{wp} takes on the larger of two values of airfoil r.m.s. response, one value corresponds to plunge response and the other to pitch response.

A large value of ϕ_{wp} is to be regarded as "bad performance" because at least one of the two displacements has a large r.m.s. value. On the other hand, a low value of ϕ_{wp} is "good performance" since both displacements are jointly small as measured by their r.m.s. values. The worst case actuator activity is defined as:

$$\phi_{wa}(\mathcal{G},\mathcal{C}) = \max(E_\infty\{z_{a1}^2(t)\}, E_\infty\{z_{a2}^2(t)\}, E_\infty\{z_{a3}^2(t)\}), \tag{8}$$

The function ϕ_{wa} is similar to ϕ_{wp}. A small value of ϕ_{wa} represents a low cost actuator set while a large value represents a "high cost" actuator arrangement. It is reasonable to assume that allowing large values of ϕ_{wa} will produce small values of ϕ_{wp}.

The ϕ functions introduced in Eqns. 7 and 8 are called "worst case figures of merit." These figures of merit are more natural and realistic design parameters than the usual "weighted sum" objective function given by

$$\psi_p(\mathcal{G},\mathcal{C}) = \lambda_1 E_\infty\{z_{p1}^2(t)\} + \lambda_2 E_\infty\{z_{p2}^2(t)\}, \tag{9}$$

where λ_1 and λ_2 are positive scalar used to assign relative importance to the individual objectives. For example, imagine that the problem is to find a controller $\mathcal{C}$ such that both $E_\infty\{z_{p1}^2(t)\}$ and $E_\infty\{z_{p2}^2(t)\}$ are below a desirable performance level. Clearly, such a feasibility problem is mathematically equivalent to the problem of minimizing (over all stabilizing controllers) the worst case figure of merit $\phi_{wp}(\mathcal{G},\mathcal{C})$ and then checking to see if the minimal worst case performance satisfies the given constraint.

On the other hand, any attempt to solve the feasibility problem by minimizing the weighted sum performance objective $\psi_p(\mathcal{G},\mathcal{C})$ first requires the selection of suitable values for the artificial parameters λ_1 and λ_2, which have little physical meaning. In addition, the problem of weight selection becomes more complicated if not impossible when we add more performance variables and we include the actuator variables in the definition of the weighted sum performance objective $\psi_p(\mathcal{G},\mathcal{C})$.

Tradeoff surfaces

To assess the advantages or limitations of different structural parameters (different plants $\mathcal{G}$ with different physical features) for the problem of gust alleviation we need to introduce a quantitative optimality concept for the cost functions ϕ_{wp} and ϕ_{wa} defined in Eqns. 7 and 8, respectively.

Since smaller values of the figure of merit functions $\phi_{wp}(\mathcal{G},\mathcal{C})$ and $\phi_{wa}(\mathcal{G},\mathcal{C})$ are better, a plant-controller pair is a "good" pair if both worst case objectives are jointly small. Now, suppose that the plant $\mathcal{G}$ is fixed (the design of the airfoil with its actuators is fixed, but the control law relating actuators output to sensor input is not). Then, given two numbers γ_1 and γ_2 (representing performance and actuator r.m.s. limits, respectively) we say that the design specification (γ_1, γ_2) is achievable if we can find a stabilizing controller $\mathcal{C}$ such that we have

$$\phi_{wp}(\mathcal{G},\mathcal{C}) \leq \gamma_1 \text{ and } \phi_{wa}(\mathcal{G},\mathcal{C}) \leq \gamma_2. \tag{10}$$

From this equation it is clear that the set of achievable specifications (γ_1, γ_2), which will be denoted by $\mathcal{A}(\mathcal{G})$, is given by the equation

$$\begin{aligned} \mathcal{A}(\mathcal{G}) \;=\; & \{(\gamma_1,\gamma_2) : \text{ there exists a stabilizing controller } \mathcal{C} \text{ such that } \phi_{wp}(\mathcal{G},\mathcal{C}) \leq \gamma_1 \\ & \text{and } \phi_{wa}(\mathcal{G},\mathcal{C}) \leq \gamma_2\}. \end{aligned} \tag{11}$$

Although cast in terms of control terminology Eqn. 11 is central to the appreciation of the power of this approach. Note that there exists at least one controller $\mathcal{C}$ such that the controlled structure satisfies a given design specification if and only if this specification belongs to the set of numbers $\mathcal{A}(\mathcal{G})$. Note also that this set is a function of the airfoil/actuator plant $\mathcal{G}$ only. (This explains our notation in Eqn. 11.) For instance, if some of the structural parameters are changed, i.e. the plant $\mathcal{G}$ is changed, then a design specification that was originally not achievable could become achievable with some stabilizing controller.

$A(\mathcal{G})$ defines a design space and the lower boundary of $\mathcal{A}(\mathcal{G})$ is called the "tradeoff surface" or the set of Pareto optimal specifications corresponding to the cost functions ϕ_{wp} and ϕ_{wa}. The tradeoff surface is a very important feature in multiobjective optimization because it determines the boundary between achievable and not achievable design specifications–i.e. the limits of achievable performance.

An example of the trade-off surface concept to illustrate its use is shown in Figure 4. This figure plots limiting combinations of γ_1 and γ_2 computed for two slightly different plant-actuator-sensor combinations. Two curves are shown in Figure 4, because there are two different plants (controlled structure configurations) to be compared.

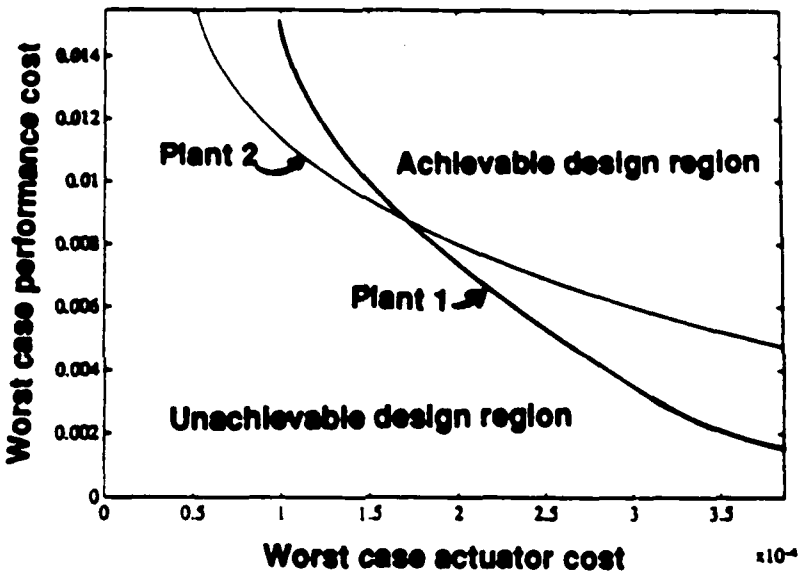

Figure 4: Typical trade-off surface (curves), showing feasible and nonfeasible regions for two different plants.

For each plant, combinations of worst case performance (γ_1) and worst case actuator cost (γ_2) lying below each curved line are not possible unless some feature of the system is changed. This change might be relocation of an actuator, resizing of an actuator, changing the stiffness of the airfoil or changing the actuator material. Note that these two trade-off curves intersect. This means that, for one range of performance requirements, one plant configuration is better than the other.

Trade-off surfaces are also valuable once control laws are proposed. The tradeoff surface may be used as an absolute measure against which different control laws can be compared. Thus, the limits of achievable performance are valuable not only to determine which struc-

tural configuration is easier to control but also they provide the necessary information to evaluate candidate controller designs with respect to the figures of merit of interest.

The methodology to compute trade-off surfaces (in our case these are 2-dimensional so they become trade-off curves) for the figures of merit ϕ_{wp} and ϕ_{we} is taken from [4] and [5]. For an exposition of the area of multiobjective control see [3]. See also [6] for some more recent work in this field. It is important to note that these trade-off surfaces are computed under the only assumption that the controllers to be used are linear and time-invariant. No other restriction on the structure of the controllers (i.e. the order of the controllers should be bounded, the controllers should have a specific architecture such as observer-based, etc.) are imposed. This means that if a design specification (γ_1, γ_2) lies below a curved line in Figure 3, there is no stabilizing controller (even infinite-dimensional) that can achieve this specification.

While the mathematical theory to create trade-off surfaces has been well developed in the above references, the programming of the numerical procedure requires time and skill. A preliminary version of the software utilized in this work may be found in [5]. This software makes use of commercial tools for control systems analysis and design, and finite dimensional convex optimization algorithms. This preliminary software package has been implemented in Matlab. The numerical methods used not only provide, to any desired degree of accuracy, points in the trade-off surface but also controllers whose cost values are as close as desired to the trade-off surface.

Numerical examples

In this section a tradeoff surface between the performance cost (measured in terms of worst case r.m.s. airfoil response in pitch or plunge) and the actuator cost (measured in terms of its r.m.s. value) is computed for three different cases. In each case, the plants use a different actuator. This simple problem will illustrate the features and value of our approach. We will conclude that the torsional spring actuator g is the best actuator signal, if only one actuator can be used, for the gust alleviation problem at an airspeed larger than the open-loop flutter speed.

The closed-loop design airspeed is set to 10% above the airfoil uncontrolled flutter speed. The weights for the performance variables z_p and the actuator variables z_a defined in Eqns.

differently. For the bending strain actuator k (dashed) we plot ϕ_{wp} vs. $\phi_{wa} = E_\infty\{z_{a1}^2(t)\}$. For the torsion strain control g (solid) we plot ϕ_{wp} vs. $10\,\phi_{wa} = 10\,E_\infty\{z_{a2}^2(t)\}$. Finally, for the trailing edge flap control (dashdot) we plot ϕ_{wp} vs. $0.1\,\phi_{wa} = 0.1\,E_\infty\{z_{a3}^2(t)\}$. The torsion strain actuator g is seen to be the most effective for all possible performance values.

The second example uses a gust scale length $L = 10\,b$ but keeps all other parameters fixed. This results in the Dryden transfer function having bandwidth on the order of the open loop torsion resonant frequency. For example, $\tau = 0.07726$ sec. and $\omega_\alpha \tau = 3.863$, so that ω_α is of the same order of the corner frequency of the Dryden transfer function.

Figure 6 shows the tradeoff surface between the worst case performance index ϕ_{wp} and the worst case actuator index ϕ_{wa} for the torsion and bending strain controls g and k. As before, we plot ϕ_{wp} vs. $\phi_{wa} = E_\infty\{z_{a1}^2(t)\}$ for the bending strain actuator k (dashed) and ϕ_{wp} vs. $10\,\phi_{wa} = 10\,E_\infty\{z_{a2}^2(t)\}$ for the torsion strain control g (solid). Clearly, torsion strain control is more effective than bending strain control.

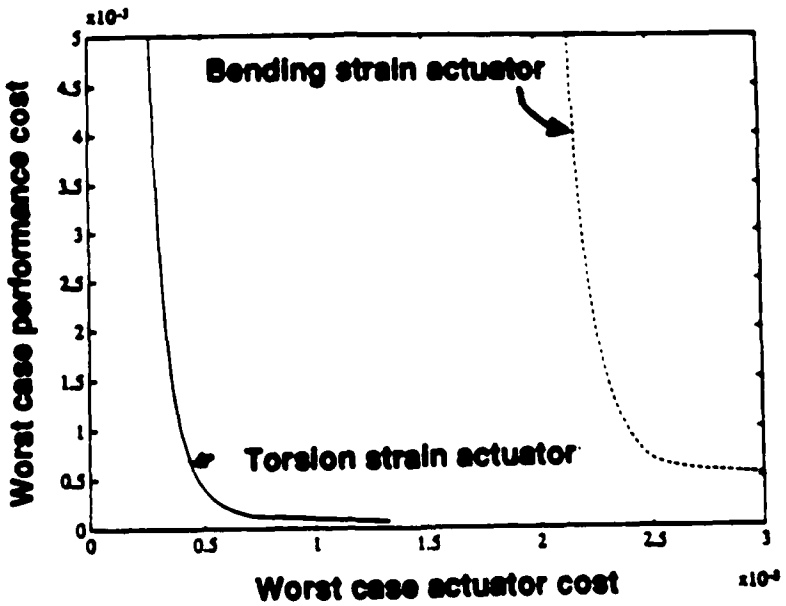

Figure 6: Trade-off surface for active material bending and torsion control.
Gust scale = 10 b.

Finally, in Figure 7, we compare trailing edge flap control (dashdot) with bending strain control (dashed). This plot does not use scaling so that actual costs are shown. It is again obvious that the active strain control is better than the trailing edge flap control in these cases.

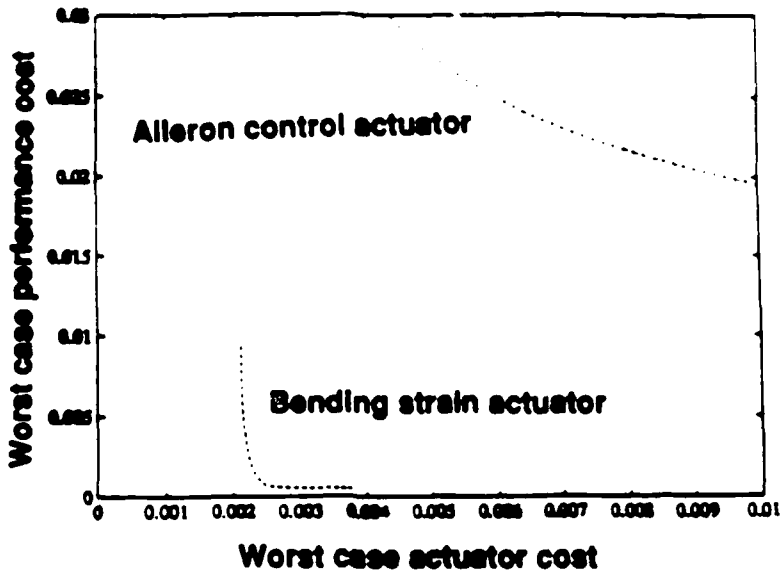

Figure 7: Trade-off surface for active bending control and aileron control.

Future efforts and summary

The work thus far has concentrated on developing a pilot program method to evaluate actuator/structure aeroelastic control effectiveness so that the effectiveness of integrated active material actuators can be predicted. By any measure, this effort has been a success. However, if the method is to have an impact of the controlled structure community, it will have to be demonstrated for a more elaborate analytical model where additional design parameters can be exposed.

At the present time a new aeroelastic model is being developed to simulate a closed-cell box beam structure with embedded piezoelectric elements. This finite element model contains unsteady aerodynamic lags and actuator dynamics. The finite element model will be more useful in the assessment of actual active material capabilities and actuator placement and sizing. Additions to the present trade-off surface software and the study of trade-off surfaces for other figures of merit of practical significance are necessary. Other figures of merit we plan to consider include the maximum time-domain excursion of the signals of interest in response to fixed or worst case exogenous inputs.

The results of this work will be used to study active material capabilities, assess directions for improvement in this area, study sizing and placement are create data that can be used for design of future test articles.

References

[1] Weissb-ar, T.A. and Ehlers, S.M., Adaptive Aeroelastic Composite Wings–Control and Optimization Issues. *Composites*, Vol. 2, Nos. 5-7, pp. 457-476, 1992.

[2] Bisplinghoff, R.L., Ashley, H. and Halfman, R.L , *Aeroelasticity*, Addison-Wesley, Reading, Mass., 1955, pp. 533.

[3] Boyd S.P. and C. H. Barratt. *Linear controller design: limits of performance*. Prentice-Hall, New Jersey, 1990.

[4] Khargonekar P. P. and M. A. Rotea. Multiple objective control of linear systems: the quadratic norm case. *IEEE Trans. on Automat. Control*, 36, 1, 14-24, 1991.

[5] Rotea M. A. and A. M. Eudaric. Ellipsoid methods for multiobjective control with quadratic performance measures. Technical report, School of Aeronautics and Astronautics, Purdue University, in preparation.

[6] Khargonekar, P. P. and M. A. Rotea. Controller synthesis for multiple objective optimal control. *Control of Uncertain Dynamical Systems*, Editors S.P. Battacharyya and L. H. Keel, CRC Press: Boca Raton, pp. 261-280, 1991.

Appendix

Technical papers

- Active Tailoring of adaptive lifting surfaces for aeroelastic applications by M.N. Abdul-Wahed and T.A. Weisshaar, presented at the 1993 North American Conference on Smart Structures and Materials, Albuquerque, N.M., Feb. 1993

- Optimizing induced strain actuators for maximum panel deflection by T.J. Leeks and T.A. Weisshaar, presented at the AIAA Adaptive Structures Forum, Hilton Head, S.C., April 1994.

Active tailoring of adaptive lifting surfaces for aeroelastic applications

M.N. Abdul-Wahed

Faculty of Mechanical Engineering, Aleppo University
Aleppo, Syria

T.A. Weisshaar

School of Aeronautics and Astronautics, Purdue University
West Lafayette, Indiana 47907-1282

ABSTRACT

This paper discusses the development and use of an effective finite element analysis procedure to examine integrated anisotropic piezoelectric actuators for aeroelastic applications where it is essential that torsion and bending be controlled independently of one another. The finite element model consists of three-dimensional isoparametric solid elements (bricks) that allow modeling of tailored piezoelectrics with skewed actuator/sensor axes. This scheme also allows the representation of an anisotropic host structure and can account for material and stacking geometry through the element thickness. Using this finite element representation, it is shown that anisotropic piezoelectric actuators can create sufficient twisting and bending to control aerodynamic loads on a wing, although aerodynamic loads are not included in this discussion.

1.0 BACKGROUND AND PURPOSE

The purpose of this paper is to examine the action and effectiveness of adaptive material actuators when they are used to create deflections of wing structures. By effectiveness, we mean the ability to cause twist and bending deflections that will, in turn, create aerodynamic loads. Here the emphasis will be on structural deflection, not aerodynamic interactions, so no aerodynamic loads will be included.

Adaptive structures use actuators to create changes in structural design shape or damping to respond to changing mission needs and performance requirements. Actuators may be articulated mechanical devices such as ailerons and flaps or they may be "smart" materials embedded in the structure. In the case of atmospheric flight vehicles, active material actuators embedded in the structure can control structural shape and aerodynamic loads. Using sensors and feedback control algorithms, these actuators also can change wing stiffness and control the stability of an entire lifting surface to maneuver and trim an aircraft, reduce gust loads or enhance the stability of the structure. In some cases, this can be done with less weight and at reduced overall cost compared to conventional structures. At present, these concepts rely on aeroelasticity, that is, the mutual interaction between aerodynamic loads and structural deflections, to create favorable active load control.

Aeroelastic control concepts are still in their infancy, but their proposed uses are increasing rapidly with each passing year. The successful application of active materials and actuator concepts depends on: a) identification of an aeroelastic phenomenon and, (b) identification of an effective actuator arrangement to control the phenomenon. Both involve creativity and the accessibility of an effective analytical procedure. The use of actuators to control aeroelastic deformation also depends on their ability to decouple two characteristic types of deformation, bending and twist. This modal decoupling is very important to aeroelastic load control because both types of deformation create aerodynamic loads, but we may not always want these loads to occur simultaneously.

The study of aeroelastic decoupling requires an accurate analytical model, one that can model arrays of anisotropic actuators oriented at angles skewed with respect to conventional structural axes. It also requires realistic modeling of an aircraft wing structure. This model may be a plate-like configuration or the closed box-beam arrangement common to all efficient aeronautical structures.

Because of the interest in effective actuator combinations and realistic structures, a finite element method was developed to model potential structure/actuator configurations. This technique draws heavily upon previous published work by several researchers, but it extends this work to cover emerging structural configurations. This theoretical development will be reviewed and discussed in this paper.

1993 North American Conference on Smart Structures and Materials
Albuquerque, New Mexico - February 1993

We first turn our attention to a survey of previous active structures work in the area of aeroelastic and aerodynamic control. This review will help the reader to understand the types of problems that are potentially worthwhile to pursue and the difficulties applying these concepts. Having done this we summarize the finite element development and discuss illustrative examples.

1.1 Aeroelastic and aerodynamic load control

Control of aerodynamic loads and structural response of wings and other lifting surfaces is not a new concept. Proposals to control wing response, in particular gust response are over thirty years old. Ride quality enhancement was used on the B-70 Valkerie Supersonic Bomber. The same concept is used today on the B-1 bomber. to allow it to conduct low level , high speed penetration missions. The Lockheed L-1011 uses active inboard flaps to reduce the severity of turbulence on wing fatigue life and on the ride quality felt by passengers. Suppression of wing flutter, a dynamic structural instability created by unfavorable interaction between unsteady aerodynamic loads and structural vibrations, was demonstrated in the mid-1970's. This flutter suppression was possible by using feedback control to drive aerodynamic surfaces such as ailerons and leading edge slats to damp out motion.

Active materials, in particular piezoelectric material actuators, have been proposed as controllers to accomplish much the same mission as aerodynamic surfaces. How successful and in what areas these material actuators will be able to replace or augment aerodynamic controllers such as ailerons is still very much in doubt. There are advantages to creating so-called "solid state wings" that have no external hinges or mechanical devices. For military applications there is the advantage of stealth. Any gaps or openings that appear in the wing tends to increase size of the radar return from an aircraft. Another advantage is that the control is distributed over the entire wing, making control of some aeroelastic phenomena more precise. Lastly, there are some aeroelastic phenomena, such as panel flutter, for which no mechanical device is feasible.

The first attempt at aerodynamic shape control is due to Crawley, *et al.*[1] at M.I.T. They examined the effectiveness of piezoelectric actuators to create twist and camber in plate-like aerodynamic surfaces. The ability of these actuators to affect aeroelastic loads was analyzed and demonstrated in wind tunnel experiments by Lazarus and Crawley[2]. In a related study, Bohlmann and Lazarus[3] examined the response of piezoelectrically actuated flat plates in an airstream. For this latter study, piezoelectric actuation created chordwise plate curvature (which creates an equivalent angle of attack) to generate aerodynamic forces.

While early studies emphasized the ability of piezoelectric actuators only to create airloads, the essential aeroelastic feedback process was not well understood. At Purdue University, Ehlers and Weisshaar[4,5,6] formulated a simple aeroelastic model for a beam-like laminated composite wing with embedded actuators. This model captured the fundamental interactions between bending and torsional deformations and aerodynamic loads. Using this model, they showed that an aeroelastic static instability called divergence could be controlled. They also demonstrated the wing lift effectiveness (the ability to increase or decrease lift) could be changed with a simple feedback control law relating wing root bending and twisting moments and piezoelectric action. They developed aero-piezo-elastic parameters for measuring the effectiveness of actuators in creating aerodynamic loads.

Lazarus, *et al.* [7] have shown the potential benefits that may occur when aerodynamic control surfaces are replaced with strain actuation. These results are limited to simple plate configurations. Ehlers[4] has also studied ways to increase aileron effectiveness using a combination of strain actuation and ailerons.

Song, *et al.* [8] considered static aeroelastic control using a thin-walled beam structure to represent a wing structure. This formulation is important to aeroelastic control analysis because the box-beam is the preferred configuration for wing structural design, although plate models may capture most of the wing behavior when the wing is thin. Persiani, *et al.* [9] have also considered the static aeroelastic behavior of an adaptive structural box beam with composite materials. Their study used the concept of strain energy tuning.

Dynamic aeroelastic phenomena have also received attention. Lazarus, Crawley and Lin[10] showed that piezoelectric strain actuation might be a viable alternative to articulated control surfaces for flutter suppression. Panel flutter suppression has been examined by Scott[11], Abou-Amer[12], Paige[13], Hajela and Glowasky[14] and Scott and Weisshaar[15]. Panel flutter suppression with piezoelectric actuators and shape memory alloy actuators is unique in that no articulated device exists to do the same task. Heeg[16] has also demonstrated airfoil flutter control with a piezoelectric actuator device.

In all previous results, shape control of aerodynamic surfaces was based on the inherent extension/contraction ability of piezoelectric (usually piezoceramic) actuator materials. This action was used to create bending distortion of plate-like or beam-like materials, which, in turn, tend to twist the structure. This twist was made possible only if there was bending/torsion coupling in the wing structure, such as will occur if laminated composites are used or if there is geometrical bend/twist coupling in swept wing planforms.[17,18] While some of these previous studies accounted for the possibility of creating shear to cause torsion, it is generally recognized that the most popular piezoceramics are electromechanically isotropic so that shear strain generation is not possible.

Obtaining decoupled, direct control of wing twist is highly desired for aeroelastic and aerodynamic load generation. Innovative, alternative ways to create decoupled twist have been suggested by Lee[19] and Barrett.[20,21] Barrett's proposed configuration uses a directional attachment of piezoelectric strips (DAP) to channel the actuation strain into torsion. Reference 20 is among a rapidly increasing number of applications to rotorcraft noise and vibration reduction. Although this procedure has been demonstrated to be effective in wing tunnel experiments, the complexity of the DAP construction may reduce its effectiveness for actual applications.

1.2 Objectives - Independent bending/torsion control and finite element modeling

One objective of this paper is to explore alternative ways of obtaining direct actuation control of adaptive structures to create a desired mode of wing twist and bending. An active tailoring concept based on active orthotropicity of some types of piezopolymeric materials will be introduced. Until now, these piezopolymerics have been excluded from aeroelastic control applications because they are not stiff and because they require high voltages to create the electric fields necessary to be effective. However, if the applied voltage is not limited, an acceptable value of the piezoelectric effectiveness parameter defined by Crawley and DeLuis[22] can be obtained.

The unique property of electromechanical anisotropy in special kinds of PVDF piezopolymers is obtained by stretching during poling.[23,24]. This property was used for the first time by Lee and Moon[25] to design micro actuators and sensors. However, applications of PVDF to adaptive structures have been limited to shape control and its use in structural damping[26,27] and in pointing devices.[28,29,30] In all of these applications, "ordinary" PVDF with isotropic electromechanical properties was used.

Decoupled piezoelectric control and the ideas related to such control require an effective analytical model. Developing such a model is the second objective of this study. Structural models of structures with integrated actuators and sensors, bonded or embedded in the host structure, have been limited mostly to simple beam models or rectangular plates. Beam models have permitted closed-form solutions to some important, problems.[22,31]

The Rayleigh-Ritz method has also been applied to active structures.[32] This method, when used in conjunction with plate theory or beam theory can be effective. On the other hand, this procedure requires a careful choice of approximating functions and is difficult to apply to general cases with arbitrarily shaped actuators and structural planforms.

Finite element models have also been developed to analyze active structures. These efforts have fallen into two categories: (a) modeling pure piezoelectric structures for transducer/vibration studies[33,34,35,36,37]; and (b) modeling host structures with integrated piezoelectric actuators/sensors, bonded or embedded in their host structures. [38,39,40] For these latter studies, the finite element method was used only on rectangular plates, not closed thin-wall sections. More importantly, these studies also were restricted to piezoelectric actuators with isotropic electromechanical properties.

This paper outlines the development of a finite element model developed to analyze plate based structures (including box-beams) subjected to mechanical/electrical excitations. The finite element model uses a thin piezoelectric element derived from Hamilton's Principle. The theory is restricted to linear piezoelectric theory, but takes into account orthotropic mechanical and electromechanical properties of the actuators.

2.0 FINITE ELEMENT DEVELOPMENT

The purpose of this section is to review the development of the finite element model used to analyze integrated, active, piezoelectrically activated structures. This review will include development and restrictions on its use.

A piezoelectric material is a material which, when subjected to mechanical load, develops an electric charge proportional to the resulting mechanical stress. Conversely, this material will deform or strain when an electric field is applied. This deformation, in particular positive or negative strain, depends on the polarity of the applied field. The electric field is generated by imposing a voltage across the material so that the field is proportional to the applied voltage divided by the distance between the electrodes.

Figure 1 (all figures have been placed at the end of this paper) represents the general type of structure to be modeled. The structure is composed of an arbitrary plate with embedded discrete piezoelectric elements. These actuator elements are poled, electroded and connected arbitrarily. The equations of motion of this continuum can be derived using a generalized form of Hamilton's principle. The variational expression for this coupled electromechanical system can be written as follows:

$$\int_{t_1}^{t_2}\left[\delta\left(T - U - W_{elec}\right) + \delta W_{ext}\right]dt = 0 \tag{1}$$

In Eqn. 1 the following definitions are used: T = *kinetic energy*; U = *potential(strain) energy*;

W_{elec} = *electrical energy*; δW_{ext} = *virtual work of external forces*.

While the expressions for the structural kinetic energy and strain energy are the standard expressions for a continuum, the electrical energy and the virtual work from the external forces include piezoelectric constitutive relations and properties.

A piezoelectric element is shown in Figure 2, together with its electrodes and coordinate axis definitions. The general properties of a piezoelectric material are defined relative to the material poling direction. This poling direction is taken parallel to the x_3 direction . We require a linear relationship between the elastic, electrical and electromechanical coupling properties of the piezoelectric material. This relationship is given by its piezoelectric-dielectric relations.[41,42] These relations read as follows:

$$\begin{Bmatrix}\{D'\}\\ \{\sigma'\}\end{Bmatrix} = \begin{bmatrix}\left[\varepsilon^S\right] & [e]\\ -[e]^T & \left[C_p^E\right]\end{bmatrix}\begin{Bmatrix}\{E'\}\\ \{S'\}\end{Bmatrix} \tag{2}$$

Equation 2 relates the electrical displacement (charge) D and the mechanical stress σ to the applied electric field, E, and the mechanical strain S through constants of proportionality representing: dielectric constants ε for the material; e, piezoelectric constants relating voltage to stress; and C_p, the piezoelectric material stiffness matrix elements. The notation $(\ )^S$ indicates that the constants are measured at constant strain (clamped), while $(\ )'$ indicates values computed in the local piezoelectric material coordinate reference frame. The superscript notation $(\ )^E$ indicates that values are measured at constant electric field (short circuited).

The relationship in Eqn. 2 can be inverted, either in its entirety or partially. In particular, the following relationship is valuable.

$$\left[d_{ij}\right] = \left[C_p^E\right]^{-1}\left[e_{ij}\right] \tag{3}$$

The elements d_{ij} are the piezoelectric charge coefficients that relate induced strain to the applied electric field. Equation 3 can be used to calculate the e_{ij} constants in terms of the d_{ij} constants, since the latter constants are generally more available than the e_{ij} constants.

2.1 Typical piezoelectric materials and properties

Table 1 summarizes some important elastic and electromechanical constants for lead zirconate titanate (PZT) and polyvinylidene fluoride (PVDF). An examination of the parameter values in this table reveals some important, essential

features of these materials. First of all, note the signs of the parameters d_{ij} in Table 1. If these coefficients are negative, the voltage must be applied in the direction opposite to the poling direction to produce positive (extensional) strains. Note also that the induced strain in PVDF is nearly uniaxial.

Piezoceramics have two orthogonal planes of symmetry., one inplane and the other out-of-plane so that, while they are orthotropic materials, there is planar isotropy in the plane perpendicular to the poling axis. This planar isotropy is evident in Table 1 for PZT where $d_{32}=d_{31}$ and $d_{24}=d_{15}$. On the other hand, piezopolymerics such as PVDF have fully isotropic structural properties, but electrically induced inplane strains that are decidedly orthotropic. Because the orthotropicity is in a plane perpendicular to the poling axis, it presents a potential for actuator tailoring.

Table 1
Piezoelectric material constants for PZT and PVDF

Property	units	PZT [43]	PVDF [24]
$E_{11}=E_{22}$	GPa	0.63×10^{11}	0.2×10^{10}
E_{33}	GPa	0.49×10^{11}	0.2×10^{10}
$G_{31}=G_{32}$	GPa	0.22×10^{11}	0.77×10^{9}
G_{12}	GPa	0.233×10^{11}	0.77×10^{9}
ν_{12}		0.35	0.3
d_{31}	m/V	$-166.\times10^{-12}$	0.23×10^{-10}
d_{32}	m/V	$-166.\times10^{-12}$	0.3×10^{-11}
d_{33}	m/V	$360.\times10^{-12}$	-0.33×10^{-10}
d_{24}	m/V	$540.\times10^{-12}$	0
d_{15}	m/V	$540.\times10^{-12}$	0
$\varepsilon_1=\varepsilon_2=\varepsilon_3$	F/M	$15.\times10^{-9}$	0.1062×10^{-9}

2.2 Inducing torsion with skewed actuators and actuator material axes

When the principal strain axes of orthotropic piezopolymers are rotated, or skewed, with respect to the host structure, we can induce shear strains. In plates or beams, this shear creates twisting of the structure. Figure 3 illustrates this behavior on a simple skewed plate. A PVDF actuator, skewed at an angle α, creates a shear stress given as:

$$\tau = \sigma_{12} = \pm V_3 \sin\alpha \cos\alpha \left(e_{31} - e_{32}\right) \tag{4}$$

This shear stress creates an equivalent shear flow in the plate, given as $q_{12} = \tau = \sigma_{12} t$. Note that, if the d_{31} and d_{32} coefficients are equal, then $(e_{31} - e_{32})$ is zero and the twisting shear flow will be zero.

Orthotropic action of actuators is essential for any successful aeroelastic control scheme. The twisting action of the actuator comes from two sources: (a) resultant, effective torque at the free end of the plate created by opposing shear flows on the upper and lower actuator elements; and, (b) differential bending applied to the two parallel free edges of the plate. The differential bending induces warping in the "correct" direction of twist.

2.3 The elemental model

The basic building block finite element model used in this study is a solid brick element, shown in Figure 4. The degrees of freedom of this element include translational displacements and electrical displacements at each node. The electrical displacements correspond to the electrical potential ϕ. There are three mechanical (translational) degrees of

freedom and one electrical degree of freedom per node and there are 8 nodes per element, as indicated in Figure 4. This element has a trapezoidal planform, with constant thickness.

The shape functions for the mechanical displacement and electrical potential fields are found in References 44 and 45. The displacement field includes degrees of freedom for incompatible modes using a "bubble function" found in Reference 46. These incompatible displacements and modes were added to avoid element locking under parasitic shear and to soften the extra thin brick element in the transverse direction. These shape functions were used to generate elemental mass, stiffness and external load matrices that were then assembled to obtain a structural equilibrium equation for the discretized structure. This equation has the following form:

$$\begin{bmatrix} [M_{uu}] & [0] \\ [0] & [0] \end{bmatrix} \begin{Bmatrix} \{\ddot{u}\} \\ \{\ddot{\phi}\} \end{Bmatrix} + \begin{bmatrix} [K_{uu}] & [K_{u\phi}] \\ [K_{\phi u}] & [K_{\phi\phi}] \end{bmatrix} \begin{Bmatrix} \{u\} \\ \{\phi\} \end{Bmatrix} = \begin{Bmatrix} \{F_m\} \\ \{F_e\} \end{Bmatrix} \tag{5}$$

where u represents mechanical nodal displacements and ϕ represents electrical displacements related to sensor output from the piezoelectric elements. The notation $\ddot{u}$ and $\ddot{\phi}$ represent differentiation with respect to time. The M_{ij} elements are inertia elements, while the K_{ij} elements are stiffness matrix elements. Equation 5 shows that there is electro-mechanical coupling in the structure. Note that no electrical "inertia" or damping is included in this model.

This finite element procedure was incorporated into a computer code that can analyze both flat plates and box-beams with rectangular cross-sections. This computer code and extensive details on the theory are included in Reference 47. This code is able to accurately model a variety of wing structural models, ranging from plates to beams to thin-wall built up structures with stiffeners. In the examples to follow, we will demonstrate some of these capabilities, together with some essential features of anisotropic actuators.

3.0 RESULTS AND DISCUSSION

To illustrate the application of the finite element model described in the Section 2.0, we have applied this method to four different cases. These cases illustrate the orthotropic actuator use and response. Case 1 examines a bimorph plate constructed of two PVDF layers so that the top layer acts as a distributed actuator while the bottom layer acts as a sensor. Case 2 is a rectangular aluminum plate sandwiched between two piezoceramic layers. Case 3 considers the same aluminum plate, but with two layers of tailored piezopolymers. Finally, Case 4 examines a steel plate sandwiched between two PVDF elements with off-axis, mirror symmetry.

Consider Case 1 with the 1 mm. thick bimorph cantilever beam constructed of two PVDF layers (with electro/mechanical properties given in Table 1), illustrated in Figure 5. The top layer acts as an actuator and the bottom layer acts as a sensor. As a result, the sensor signal (nodal electrical potential ϕ_s) is proportional to the induced mechanical strain in the bottom layer. This beam is subdivided into 20 identical finite elements. The major strain axis is aligned in the x_2 direction for both top and bottom layers so that the skew angle is 90° so that no anisotropic coupling is created.

Figure 6 shows the beam deflection and sensor output due to an electrical excitation of 1000 volts, applied across the top actuator layer. Because the actuator extends uniformly from the cantilever beam root to its tip, the effect of the actuator on the beam is the same as if a concentrated moment were applied at the tip. As a result, uniform bending, with a constant strain level occurs, as indicated by the nearly uniform sensor output shown in Figure 6. Only the beam root region, where the finite element method correctly predicts a boundary strain transition region, is the strain not uniform.

Case 2, considers a 1 mm. thick uniform aluminum plate sandwiched between two 0.25 mm. piezoceramic layers, with asymmetric poling, as shown in Figure 7. Sixty finite elements are used to capture the plate-like behavior when the two actuator layers are activated by 100 Volts, applied asymmetrically. As a result, one actuator stretches while the other contracts. As shown in Figure 8, the deflection of the plate is composed primarily of spanwise bending. However, some camber bending occurs because of the influence of d_{32}. It is impossible to generate twist with this actuator pair arranged in this way.

In an attempt to generate twist , the same host plate is activated with offset (skewed) piezoceramic elements, as shown in Figure 9. The resulting displacement, shown in Figure 10, is that a considerable amount of twist is generated, but substantial downward bending also accompanies this twist.

Case 3 uses the same host structure/actuator arrangement as shown in Figure 7, with the exception that the actuators are 0.25 mm. thick PVDF. These orthotropic PVDF layers are arranged with their major axes at 45° on the upper side and -45° on the lower side to achieve mirror symmetry of the actuator pair. When 10,000 Volts are applied to each actuator layer, the resulting displacement, shown in Figure 11, is pure twist (except in the boundary region near the root). In addition, the twisted sections do not have any chordwise deformation in the chordwise (camber) direction.

Case 4 considers a steel plate with PVDF actuators attached, as illustrated in Figure 12. The principal coordinate axes of the PVDF actuators are arranged at 45° on the top and -45° on the bottom. This configuration corresponds to one used by Barrett in Reference 21. A voltage of 32,000 volts is then applied. This voltage is large, but it represents the maximum allowable voltage per unit thickness (40 Volts/μm) that is given by the manufacturer. The resulting torsional displacement, plotted as afunction of distance from the cantilever support, is shown in Figure 13.

The tip displacement shown in Figure 13 is 5.25 degrees and is comparable to results obtained by Barrett for his EDAP construction. Despite the very large voltage used here, the simplicity of the PVDF technology may make it a candidate for twister actuators.

It is important to note the influence of the thickness of the PVDF layer. Increasing the actuator thickness will increase the induced shear flow and the induced torque, but it will also increase the torsional stiffness of the section. As a result, there will be an optimal thickness for maximum twist. In the present case, additional calculations showed this optimal actuator thickness to be about 0.8 mm.

4.0 CONCLUSION

An effective and versatile method of finite element analysis to investigate adaptive structure combinations with actuators having in-plane electromechanical orthotropicity has been outlined. This analytical procedure was used to demonstrate the ability of piezoelectric actuators to generate pure, decoupled torsion for aeroelastic control. Among the conclusions of this study are:

a) Electromechanical anisotropy is an effective and highly desirable, if not essential, to aeroelastic control. Efforts should be directed towards developing more effective anisotropic materials with larger (and unequal) strain or stress constants (d_{31} or e_{32}) and a larger modulus of elasticity.

b) The finite element method can provide an accurate solution for thin and thin-walled structures microactuated by thin piezoelectric elements. This method can readily account for the presence of webs and stiffeners, either active or passive, to study new configurations.

Future work will concentrate on using this finite element model to assess aeroelastic effects on thin plates in supersonic flow and built-up wings in transonic flow. Such configurations can be used to suppress flutter, control shock wave formation and to reduce drag. In addition, this finite element formulation can be used for optimization studies to determine effective actuator geometry and locations and to help to understand issues related to integrating these actuators with host structures.

5.0 ACKNOWLEDGMENTS

The first author gratefully acknowledges the support of the Council for International Exchange of Scholars (CIES) for the Fulbright Fellowship support received while a Visiting Professor at Purdue University. He also thanks Purdue University for their support during this time. The second author acknowledges the support of AFOSR Grant 91-0386 which made this cooperative effort fruitful.

6.0 REFERENCES

1. Crawley, E. F., Warkentin, D. J. and Lazarus, K. B., "Feasibility Analysis of Piezoelectric Devices," MIT-SSL-5-88, Space Systems Laboratory, Massachusetts Institute of Technology, Cambridge, Mass., Jan. 1988.

2. Lazarus, K. B. and Crawley, E. F., "Induced Strain Actuation of Composite Plates," GTL Report No. 197.

3. Bohlmann, J. and Lazarus, K. B., "Active Structures Technology Development," GD-ERR-FW-3064, General Dynamics Corporation, Ft. Worth, Texas, 12 Feb. 1990.

4. Ehlers, S. M., "Aeroelastic Behavior of an Adaptive Lifting Surface," Ph.D. Dissertation, Purdue University, August 1991.

5. Ehlers, S.M. and Weisshaar, T. A., "Static Aeroelastic Behavior of an Adaptive Laminated Piezoelectric Composite Wing," Proceedings of the AIAA/ASME/ASCE/AHS/ASC 31st Structures, Structural Dynamics, and Materials Conference, Part III, pp. 2340-2350, Long Beach, Calif., April 1990.

6. Weisshaar, T. A., Ehlers, S. M., "Adaptive Static and Dynamic Aeroelastic Design," Proceedings of the 1991 International Forum on Aeroelasticity and Structural Dynamics, Workshop on Smart Material Systems and Structures, Aachen, Germany, June 1991.

7. Lazarus, K. B., Crawley, E. F. and Bohlmann, J.., "Static Aeroelastic Control Using Strain Actuated, Adaptive Structures," Proceedings of the First Joint U.S./Japan Conference on Adaptive Structures, Maui, Hawaii, October, 1990.

8. Song, O., Librescu, L., Rogers, C. A., "Static Aeroelasticity Behavior of Adaptive Aircraft Wing Structures Modeled as Composite Thin-Walled Beams," International Forum on Aeroelasticity and Structural Dynamics, Aachen, Germany, June 1991.

9. Persiani, F., Santini, P., and Saggiani, G. M., "Parametric Aeroelastic Analysis of Composite Wing Boxes with Active Strain Energy Tuning," Presented at the ICAS Conference, Beijing, China, September 1992.

10. Lazarus, K. B., Crawley, E. F., and Lin, C. Y., "Fundamental Mechanisms of Aeroelastic Control with Control Surface and Strain Actuation," Proceedings of the 32nd AIAA/ASME/ASCE/AHS Structures, Structural Dynamics and Materials Conference, Baltimore, Md., April 1991.

11. Scott, R.C., "Control of Flutter Using Adaptive Materials," M.S. Thesis, Purdue University, West Lafayette, Indiana, May 1990.

12. Abou-Amer, S.A., "Control of Panel flutter at High Supersonic Speed," Ph.D. Dissertation, Illinois Institute of Technology, Chicago, Ill., Dec. 1991.

13. Paige, D., "Active Control of Composite Panel Flutter Using Piezoelectric Materials," M.S. Thesis, Purdue University, West Lafayette, Indiana, May 1992.

14. Hajela, P. and Glowasky, R., "Application of Piezoelectric Elements in Supersonic Panel Flutter Suppression," AIAA Paper No. 91-3191, AIAA/AHS/ASEE Aircraft Design Systems and Operations Meeting, Baltimore, Md., Sept., 1991.

15. Scott, R. C. and Weisshaar, T. A., "Controlling Panel Flutter Using Adaptive Materials," Proceedings of the 32nd Structures, Structural Dynamics and Materials Conference, Baltimore, Md., April 1991.

16. Heeg, J., "An Analytical and Experimental Investigation of Flutter Suppression via Piezoelectric Actuation," AIAA Paper No. 92-2106-CP.

17. Shirk, M. H., Hertz. T. J., and Weisshaar, T. A., "Aeroelastic Tailoring - Theory, Practice, and Promise," *Journal of Aircraft*, Vol. 23, No. 1, Jan. 1986, pp. 6-18.

18. Weisshaar, T. A., "Aeroelastic Tailoring: Creative Use of Unusual Materials," AIAA Paper No. 87-0976-CP, 28th AIAA/ASME/AHS/ASCE Structures, Structural Dynamics and Materials Conference, Monterey, Calif., April 1987.

19. Lee, C.K., "Piezoelectric Laminates for Torsional and Bending Modal Control: Theory and Experiment," Ph.D. Dissertation, Cornell University, Ithaca N.Y., May 1987.

20. Barrett, R., "Intelligent Rotor Blade Actuation Through Directionally Attached Piezoelectric Crystals," Presented at The American Helicopter Society National Forum, Washington, D.C., May 1990.

21. Barrett, R., "Active Plate and Missile Wing Development Using EDAP Elements," Presented at the Third International Conference on Adaptive Structures, November 9-11, 1992, San Diego, CA.

22. Crawley, E. F. and De Luis, J., "Use of Piezoelectric Actuators as Elements of Intelligent Structures," *AIAA Journal*, Vol. 25, No. 10, pp. 1373-1385.

23. Fukada, E. and Furukawa, T., "Piezoelectricity and Ferroelectricity in Polyvinylidene Fluoride," *Journal of Ultrasonics*, pp. 31-39, Jan. 1981.

24. KYNAR Piezo Film Technical Manual, Penwalt, Valley Forge, N.Y., 1987.

25. Lee, C. K., Moon, F. C., "Laminated Piezopolymeric Plates for Torsion and Bending Sensors and Actuators," *Journal of the Acoustical Society of America*, 85(6), June 1989.

26. Bailey, T. and Hubbard, J. E., "Distributed Piezoelectric - Polymer Active Vibration Control of a Cantilever Beam," *Journal of Guidance, Control and Dynamics*, Vol. 8, No. 5, Sept.-Oct. 1985.

27. Tzou, H. S. and Gadre, M., "Theoretical Analysis of a Multi-Layered Thin Shell Coupled with Piezoelectric Shell Actuators for Distributed Vibration Controls," *Journal of Sound and Vibration* (1989), 132(3), 433-450.

28. Baier, H., "On Shape Control of Precision Structures: Concepts, Analysis, Technology," Presented at International Forum on Aeroelasticity and Structural Dynamics, Aachen, Germany, June 1991.

29. Tzou, H. S., "Development of a Light Weight Robot End Effector Using Polymeric Piezoelectric Bimorph," Proceeding of the 1989 IEEE International Conference on Robotics and Automation, Scotsdale, Ariz., May 14-19, 1989.

30. Jiang, Z. W., Chonan, S., Abe, H., and Tani, J., "Position Control of a Flexible Arm Using Piezoelectric Bimorph Cells," *Journal of Dynamic Systems, Measurement and Control*, Vol. 113, June 1991, pp. 327-329.

31. Wang, B. T. and Rogers, C. A., "Modeling of Finite Length Spatially-Distributed Induced Strain Actuators for Laminate Beams and Plates," *Journal of of Intelligent Material Systems and Structures*, Vol. 2, January 1991.

32. Crawley, E. F. and Lazarus, K. B., "Induced Strain Actuation of Isotropic and Anisotropic Plates," AIAA Paper No. 89-1326-CP.

33. Alik, H. and Hughes, T.J.R., "Finite Element Method for Piezoelectric Vibration," *International Journal of Numerical Meth.ods in Engineering*, Vol. 2, 151-157, 1970.

34 Alik, H. and Webman, K. M., "Vibrational Response of Sonar Transducers Using Piezoelectric Finite Elements," *Journal of the Acoustical Society of America* Vol. 6, No. 6, December 1974.

35. Nailon, M., Coursant, R. H., and Besnier, F., "Analysis of Piezoelectric Structures by a Finite Element Method," *Acta Electronica*, 25, 4, 1983, pp. 41-362.

36. Lerch, R. and Kaarman, H., "Three-Dimensional Finite Element Analysis of Piezoelectric Media," Proceedings of the 1987 IEEE Ultrasonic Symposium, pp. 853-858.

37. Ostergaard, D. F. and Pawlak, T. P., "Three-Dimensional Finite Elements for Analyzing Piezoelectric Structures," Proceedings of the 1986 IEEE Ultrasonic Symposium, Williamsburg (639).

38. Tzou. H. S. and Tseng, C. I., "Distributed Piezoelectric Sensor/Actuator Design for Dynamic Measurement/Control of Distributed Parameter Systems: Piezoelectric Finite Element Approach," *Journal of Sound and Vibration* (1990) 138(1), 17-34.

39. Ha, S. K., Keilers, C., and Chang, F. K., "Analysis of Laminated Composites Containing Distributed Piezoelectric Ceramics," *Journal of Intelligent Materials, Systems and Structures*, Vol. 2, January 1991.

40. Rao, S. S. and Sunar, M., "Distributed Thermopiezoelectric Sensors and Actuators in Structural Design," AIAA Paper No. 92-2523-CP.

41. Jaffe, B., Cook, R., and Jaffe, H., Piezoelectric Ceramics, Academic Press, New York, NY 1971.

42. IEEE Standard 176-1978, "IEEE Standard on Piezoelectricity," 1978.

43. Piezo Systems Product Information, Piezo System, Inc., Cambridge, Massachusetts.

44. Bath, K. J., Finite Element Procedures in Engineering Analysis, Prentice-Hall, Englewood Cliffs, NJ, 1982.

45. Cook, R. D., Concepts and Applications of Finite Element Analysis, Third Edition, John Wiley & Sons, New York, 1989.

46. Wilson, E. L., Taylor, R. L., Doherty, W. P., and Ghabousi, J., "Incompatible Displacement Models," Numerical and Computer Methods in Structural Mechanics, Academic Press, New York, 1973, p. 43.

47. Abdul-Wahed, M.N., "Finite Element Modeling for Piezoelectric Structures," AAE Aeroelasticity Report 92-5, School of Aeronautics and Astronautics, Purdue University, West Lafayette, Indiana, August 1992.

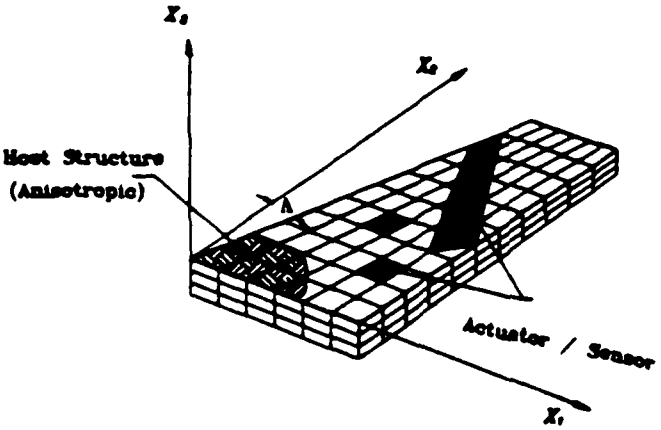

Figure 1 - Adaptive structure finite element discretization with sensors/actuators.

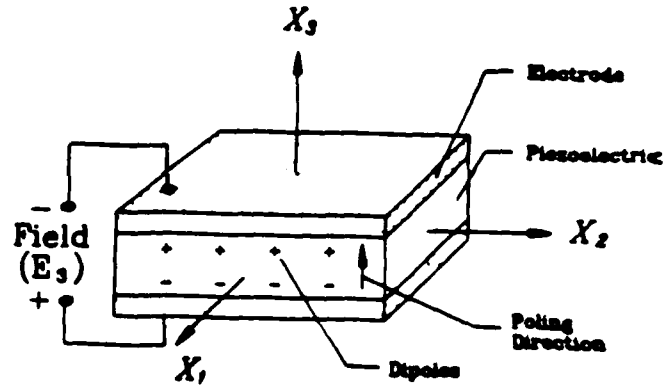

Figure 2 - Piezoelectric element with electrodes, showing coordinate axes.

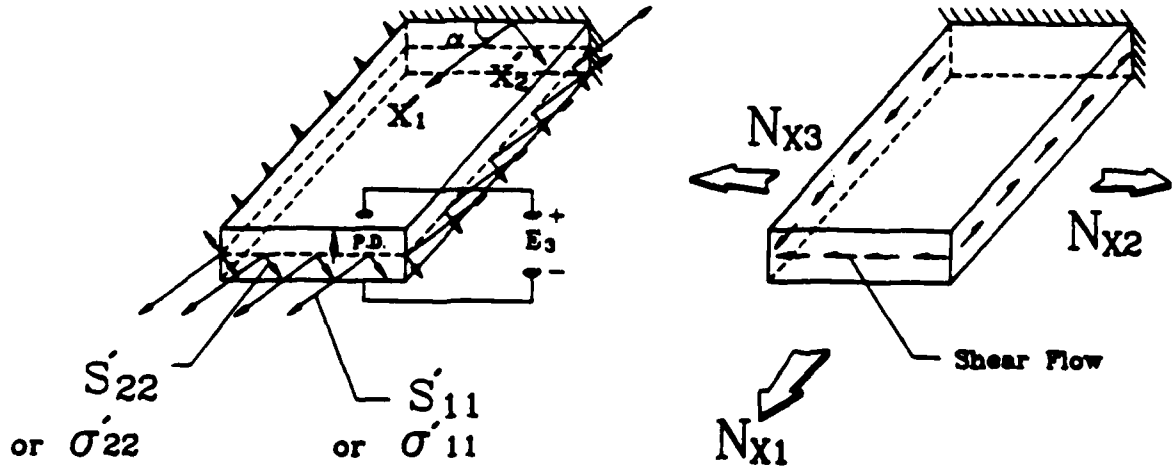

Figure 3 - Skewed PVDF actuator with inplane normal stresses and shear resultants.

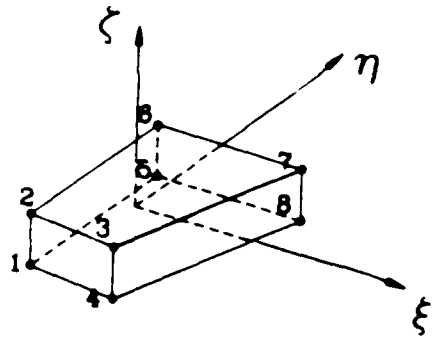

Figure 4 - 8 node trapezoidal brick element, showing local axis system.

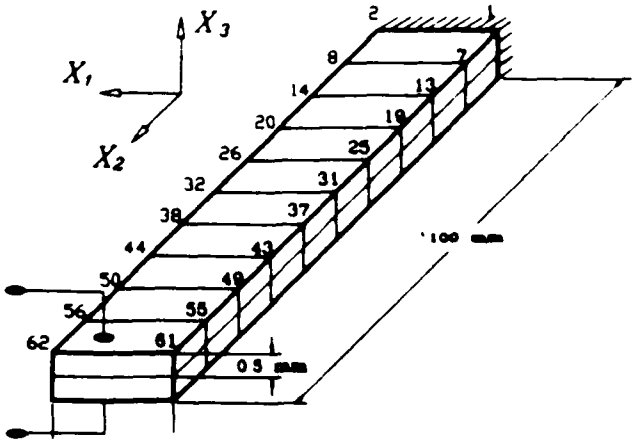

Figure 5 - Bimorph piezoelectric beam with two PVDF layers (100mmx10mm).

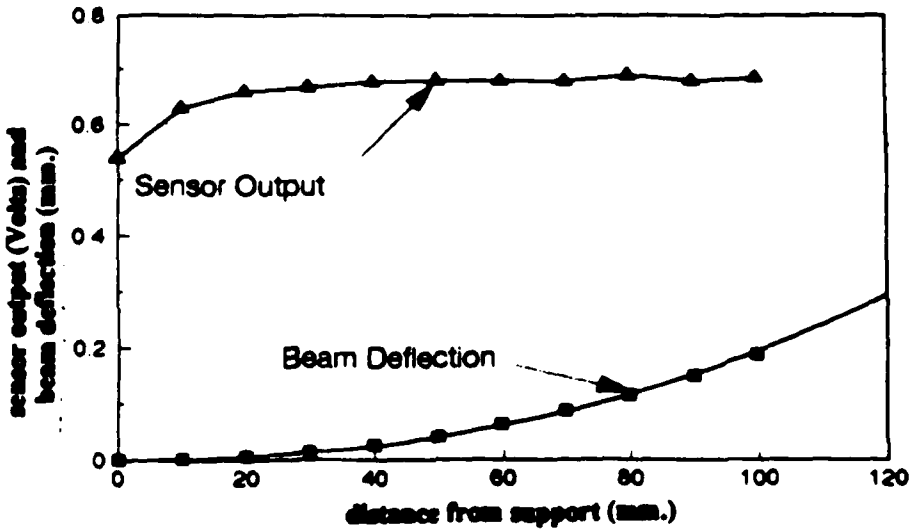

Figure 6 - Bimorph PVDF beam centerline displacement and sensor output due to 1000 Volt excitation.

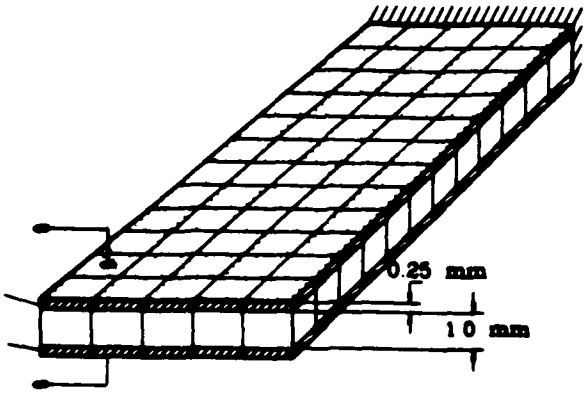

Figure 7 - Cantilever aluminum host plate with asymmetrical PZT actuator layers.

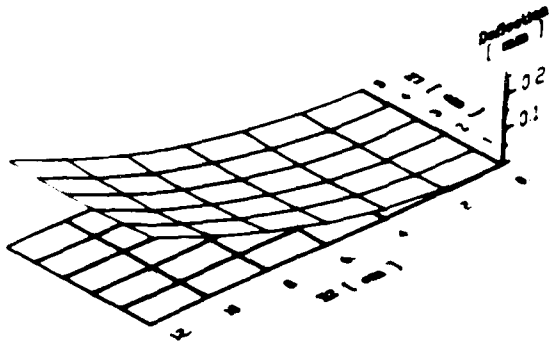

Figure 8 - Deformation pattern for Case 2 actuated PZT/aluminum beam.

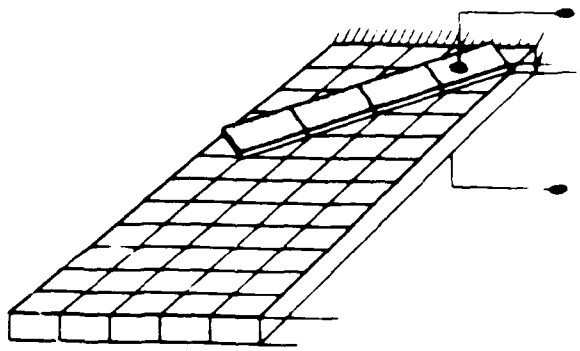

Figure 9 - 1 mm. thick aluminum cantilever beam with skewed 0.5 mm. thick PZT actuator array.

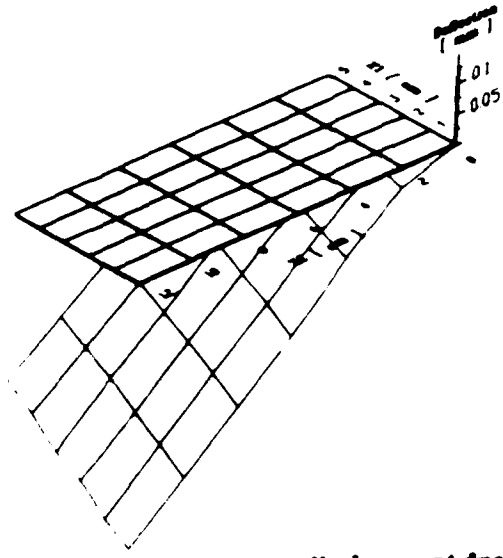

Figure 10 - Cantilever plate displacement due to skewed PZT actuator array.

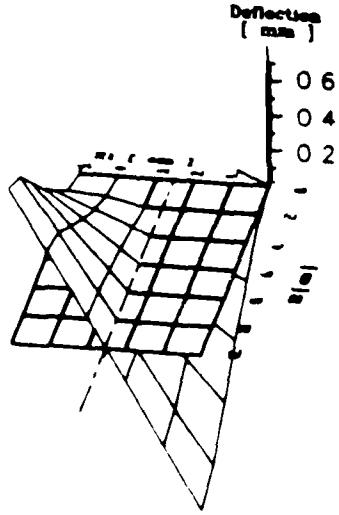

Figure 11 - Cantilever plate deformation due to skewed axis PVDF actuator excitation.

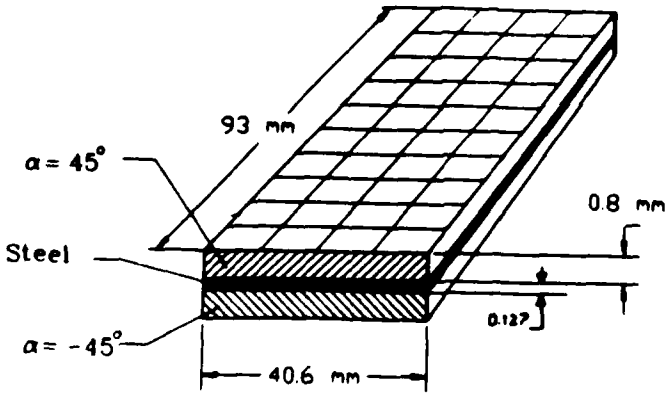

Figure 12 - Cantilever steel plate with skewed axis PVDF actuators attached.

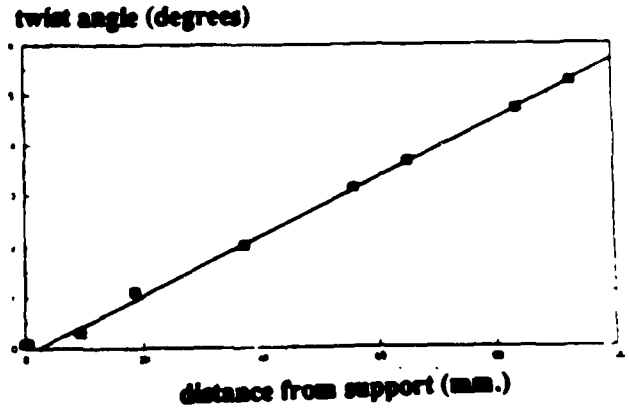

Figure 13 - Torsional displacement of steel cantilevered plate/PVDF due to 32,000 volt excitation.

OPTIMIZING INDUCED STRAIN ACTUATORS FOR MAXIMUM PANEL DEFLECTION

Tamara J. Leeks*

Terrence A. Weisshaar**

Purdue University
West Lafayette, Indiana

Abstract

This paper examines the electro-mechanical interaction between a thin self-straining piezoelectric actuator and a simply supported host plate when the actuator is placed on one side of the plate and its objective is to create a large bending deflection. The purpose of the actuator is to create bending deflections to control local aerodynamic pressures and resultant forces such as lift and drag. These studies show that there is a trade-off between the additional stiffening, provided by actuator thickness and the area that it covers on the plate, and the amount of force and moment provided by the actuator. A Rayleigh-Ritz analysis shows that the optimum size, thickness and coverage, of the actuator with respect to the host panel is determined by panel aspect ratio, and relative elastic moduli. The strain energy content of the actuator/plate combination shows that the best combinations of actuator thickness and panel coverage can be identified by plotting strain energy against actuator thickness or area. With an aluminum host plate and a PZT actuator, the best rectangular actuator size is about 0.6 the thickness of the plate and covers about 65% of the host plate.

Introduction

Aerodynamic loads, and the local pressures that create these loads, depend on the surface shape on which they act. Surface panels may be flat or curved and are designed to provide aerodynamic shape and to guarantee structural integrity. Re-shaping smooth aero/structural surfaces to change the pressure distribution is done by bonding or otherwise attaching thin actuators to the inside surfaces of structural panels to create an asymmetric configuration that will bend on command.

Thin plate-like or lattice reinforced panels with embedded self-straining actuators such as shape memory materials or piezoelectric materials have been proposed for aerodynamic control concepts that include actively controlled panels to reduce transonic drag[1,2] and active panel elements to increase supersonic panel flutter speed [3,4,5,6,7]. For transonic drag reduction, the deformation of a panel on the upper surface of a supercritical airfoil can change the flow field and shock wave intensity to reduce drag on command.

Panel flutter suppression with piezoelectric actuators and shape memory alloy actuators is unique in that no articulated device exists to do the same task. In supersonic flow, dynamic oscillations can be reduced by placing thin actuators on the panel surfaces to change the frequencies of the panels on command.

One serious problem with active panel concepts is the difficulty finding a design combination to give large enough panel out-of-plane deformations to create the required changes in aerodynamic forces. Without deflections of the order of a panel thickness (or even more), controlling the size and position of the aerodynamic forces is marginal.

A desirable actuator, such as one using today's piezoelectric materials, can not create significant bending deformation of panels unless the host panel/actuator combination is tailored to extract every bit of electro-mechanical efficiency out of the configuration. An emphasis on efficiency naturally leads to considerations of formal optimization that includes a design objective and design variables. However, before formal optimization can proceed, we must select our design variables and determine the sensitivity of the design objective to these design variables.

This paper is a pre-optimization study that examines the interaction between actuator self-straining ability, bending stiffness, thickness and planform coverage and the host panel bending stiffness and aspect ratio. The purpose of the actuator is to produce large bending deflection. The intent of the study is to identify effective panel/actuator combinations and understand why some combinations are more effective than others.

Background and configuration description

Parameters that affect panel out-of-plane deflection and enter into the optimization process include: the thickness of the actuator compared to the thickness of the panel; the surface area covered by the actuator; the position of the actuator on the panel surface; the boundary conditions at the edges of the panel; the aspect ratio of the panel planform; and, the material properties of the actuator compared to the host panel.

Analytical work described in this paper uses a baseline configuration shown in Figure 1. The size of this panel is consistent with the requirements for an active panel that might be placed between ribs of an active wing. The host plate material is aluminum, with dimensions of 12 in. by 18 in., and a thickness of 0.05

* NSF Graduate Research Fellow, School of Aeronautics and Astronautics, Member AIAA

** Professor, School of Aeronautics and Astronautics, Fellow AIAA

in. A thin lead zirconate titanate (PZT) piezoelectric actuator is attached to the bottom inner surface of the host plate. Expansion or contraction of this actuator will cause panel extension and bending. The area and thickness of the actuator are parameters for the study.

Kim & Jones[8] have studied a similar problem to find the optimal thickness of piezoactuators to maximize the bending moment induced by rectangular actuators surface-bonded to the upper and lower surfaces of a thin flat plate. They found that the best actuator thickness is approximately half the thickness of a steel host substructure and a quarter of the thickness for an aluminum host substructure.

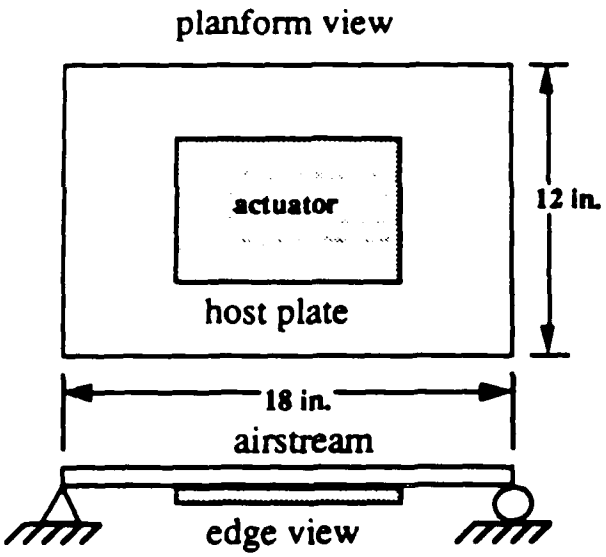

Figure 1 - Panel/actuator geometry

Rogers, Liang, & Jia[9] studied mid-plane symmetric shape memory alloy reinforced plates, using a Rayleigh-Ritz method for their numerical results. They obtained an approximate solution to the plate bending problem, free vibration, buckling, and acoustic transmission loss.

Crawley & Lazarus[10] developed a consistent plate model with embedded actuator stiffness and strain included as laminated plate layers. Their computations were based on a Rayleigh-Ritz model. Wang & Rogers[11] also applied laminate plate theory to a laminated plate containing induced strain actuator "patches" bonded symmetrically to the surface or embedded within the laminate. The thickness and size of these actuator patches are relatively small compared to those of each lamina.

This study differs from previous studies because the actuator is placed on only one side of the host plate. However, we will use laminated plate theory and a Rayleigh-Ritz solution technique, although we will check its accuracy using a finite element analysis.

Unsymmetric host plate/actuator combinations are different than symmetrical combinations in at least two major ways. First of all, nonsymmetry of the material stiffness through the thickness of the plate/actuator combination assures that there will be coupling between in-plane induced strain and panel bending. The bending stiffness of the plate/actuator combination will always be less than a similar combination of material where the total actuator thickness is the same, but distributed symmetrically about the mid-plane[12].

There is a second major difference between our configuration and symmetrical panel actuator combinations. For unsymmetric cross-ply laminates, "large deflection effects" can occur for configuration loading that normally would be regarded as producing deflections in the small plate deflection range. Bending-extension coupling can produce a stiffening or softening effect depending on the direction of the deflection.[13] An unsymmetric cross-ply laminate in cylindrical bending has different apparent bending stiffnesses in the positive and negative deflections. As a result, positive and negative loads of the same magnitude produce different magnitudes of deflection and linear lamination theory may give large differences when the nonlinear effects are ignored.[14]

Nonlinear large deflection effects will most likely increase the bending deflection found from linear theory. Our intent is to provide information as how to maximize panel bending deflections. The additional computational effort required to consider these nonlinearities was not regarded as essential to these results at this time, so nonlinear effects were excluded from this study.

Two computational methods for calculating bending deflection were considered. A finite element program (NASTRAN) was first used to compute the deformations of the plate/actuator combination. In addition, a Rayleigh-Ritz procedure was developed, beginning with a strain energy expression based on laminated plate theory. This expression and the development of the equations of static equilibrium necessary to compute bending deflection are provided in the Appendix. The analysis is based on classical laminated plate theory. The energy expression is useful as a guide to understanding why some plate/actuator combinations are better than others.

Finite Element Model

The panel configuration modeled using the NASTRAN finite element program consisted of quadrilateral plate elements with membrane and bending stiffness. Each of the small elements has the same aspect ratio as the plate, and are arranged 24 along each side, for a total of 576 elements. The actuator elements are directly attached to the host plate with no intervening bonding layer.

For each different actuator/host plate configuration considered, a new model must be created and the finite element program run. While the model computation time is small, the time required to create models and to interpret data was considered to be excessive, given the scope of our study.

The piezoelectric strain is a combination of the piezoelectric constant d_{31} multiplied by the electric field strength E_3. NASTRAN has no piezoelectric finite element capability, so an equivalent thermal element was used. Thermal and piezoelectric strains are both induced strains so that a thermal coefficient of expansion and temperature increase can be assigned to mimic the actuation strain of the piezoelectric material.

Rayleigh-Ritz Approach

An approximate solution for the plate deflections can be obtained using a Rayleigh-Ritz method based on laminate electro-mechanical strain energy and an assumed displacement field for inplane and out-of-plane (bending) deflections. The panel strain energy expression in the Appendix is composed of four basic types of terms and may be written conceptually as:

$$U = \textit{inplane stiffness} + \textit{bending stiffness}$$
$$+ \textit{inplane / bending coupling} + \textit{induced strain}$$

The stiffnesses involving shear-extension coupling vanish if the laminate is a symmetric laminate with isotropic or specially orthotropic layers, that is

$$A_{16} = A_{26} = B_{16} = B_{26} = D_{16} = D_{26} = 0 \qquad (1)$$

The assumed displacements must satisfy the simply-supported plate edge boundary conditions. Two approximate solutions were used. The first is a single polynomial term (a true Rayleigh solution), while the other is a more general series solution (a Ritz solution).

When the actuator is restricted to be at the plate center, a single set of three polynomial assumed displacements, with their origin at the center of the plate, is

$$u_o = A\frac{x}{a} \qquad v_o = B\frac{y}{b} \qquad (2)$$

$$w = C\left(1-\frac{x^2}{a^2}\right)\left(1-\frac{y^2}{b^2}\right) \qquad (3)$$

where u, v and w are the inplane displacements in the x,y and bending directions, respectively.

A more general assumed displacement set is[15]

$$u_o = \sum_{m=1}^{M}\sum_{n=1}^{N} A_{mn}\cos\frac{m\pi x}{a}\sin\frac{n\pi y}{b} \qquad (4)$$

$$v_o = \sum_{m=1}^{M}\sum_{n=1}^{N} B_{mn}\sin\frac{m\pi x}{a}\cos\frac{n\pi y}{b} \qquad (5)$$

$$w = \sum_{m=1}^{M}\sum_{n=1}^{N} C_{mn}\sin\frac{m\pi x}{a}\sin\frac{n\pi y}{b} \qquad (6)$$

The reader should note that the deflection coefficients A_{mn} and B_{mn} in Eqns. 4 and 5 are not the same as the laminate stiffness coefficients in Eqn. 1.

When either of the assumed displacement expressions are substituted into the strain energy expression, the Principle of Virtual Work can be used so that the strain energy is minimized with respect to the displacement coefficients. A set of linear equations of static equilibrium results.

When the polynomial deflection is used, this energy minimization results in only three equilibrium conditions for the constants A, B and C, given as follows

$$\frac{\partial U}{\partial A} = 0 \qquad \frac{\partial U}{\partial B} = 0 \qquad \frac{\partial U}{\partial C} = 0 \qquad (7)$$

This set of three simultaneous equation sets must be solved for the deflection coefficient sets A, B, and C. These coefficients are then substituted into the displacement equations to find the plate deflection at the center of the plate.

If only bending of the plate is considered, and the inplane energy and inplane-bending coupling energy is ignored, the strain energy expression contains only bending stiffness matrix terms and the induced piezoelectric moments. To solve for the deflections, only the third of the polynomial equations is substituted into the energy expression. While this reduces the workload, it leads to errors. The coupling terms are very important.

There are differences between retaining the inplane stiffness and inplane/bending stiffness coupling terms and ignoring them. Figure 2 compares the results of the uncoupled bending analysis and the bending-extension coupling analysis using the simple polynomial expression to the finite element solution. All of the cases were run for an actuator to plate thickness ratio of 0.6.

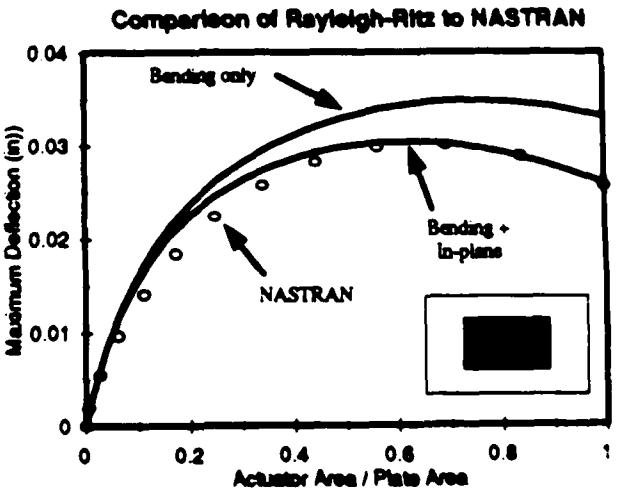

Figure 2 - Plate center bending deflection computed by Ritz method with polynomial approximation.

It can be seen that the uncoupled bending solution over predicts the deflection for the entire range of actuator area ratios, showing that it is important to include the inplane/bending coupling terms. The bending-extension coupling solution is remarkably close to the NASTRAN solution for these simple displacement functions. However, the actuator is restricted to being centered on the plate.

Because we want to assess the effects of changing the actuator location on the plate, and to get a more accurate solution, the trigonometric series displacement functions were used for tall other studies. Substituting them into the strain energy expression in the Appendix and minimizing with respect to the undetermined displacement coefficients results in the general conditions

$$\frac{\partial U}{\partial A_{mn}} = 0 \qquad \frac{\partial U}{\partial B_{mn}} = 0 \qquad \frac{\partial U}{\partial C_{mn}} = 0 \qquad (8)$$

The result is a set of $3\,M \times N$ simultaneous equations which must be solved for the series coefficients A_{mn}, B_{mn}, and C_{mn}.

The form of the equations for the displacement coefficients is

$$[K_{ij,mn}]\{A_{mn}\} = \{Q_{ij}\} \qquad (9)$$

where $[K_{ij,mn}]$ is a $(3\,M \times N)X(3\,M \times N)$ matrix of stiffness terms, found from integrating the assumed displacement series strains into the energy expression, $\{A_{mn}\}$ is a $3\,M \times N$ vector consisting of the vectors of A_{mn}, B_{mn}, and C_{mn} coefficients. $\{Q_{ij}\}$ is a $3\,M \times N$ load vector whose terms represent the induced piezoelectric forces and moments. These latter terms can be thought of as the modal forces and moments for each of the assumed displacement terms.

The stiffness matrix $[K_{ij,mn}]$ is inverted to solve for the displacement coefficients., This matrix becomes large as more terms are added to the series solution. For our results, $M = N = 11$ was used. This results in a stiffness coefficient matrix that is of order 363x363. Figure 3 shows the agreement between this series solution and the finite element results.

Effects of actuator thickness and area

Actuator thickness and area for the baseline plate in Figure 1 were varied to find an actuator/aluminum host plate combination that produced the most panel center bending deflection.

For these studies, the actuator was located at the center of the plate planform and attached to its underside. The maximum bending deflection occurred at the plate center. A range of actuator thickness to plate thickness ratios between 0.1 to 1.0 was examined. For each thickness ratio, a range of actuator planform coverage from 5% to 100% of the plate area was examined. From these results, the combination of actuator thickness ratio and area ratio that produced the largest deflection could be determined.

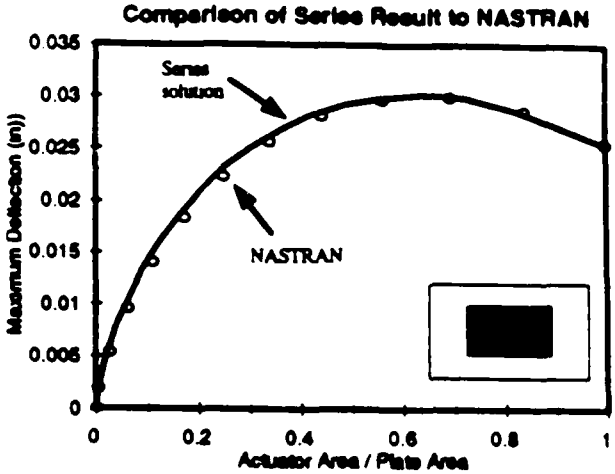

Figure 3 - Plate center bending deflection using trigonometric Ritz approximation with thickness ratio of 0.6 - comparison with NASTRAN (M=N=11)

Figure 4 shows the results of a Rayleigh-Ritz analysis to compute the panel center deflection produced by an actuator with an actuator/host plate thickness ratio between 0.1 and 0.6 for actuator/host plate area ratio between 0.1 and 1. This figure indicates that an actuator/plate thickness ratio of 0.6 produces the largest panel deflection when the actuator/plate area ratio is 65%.

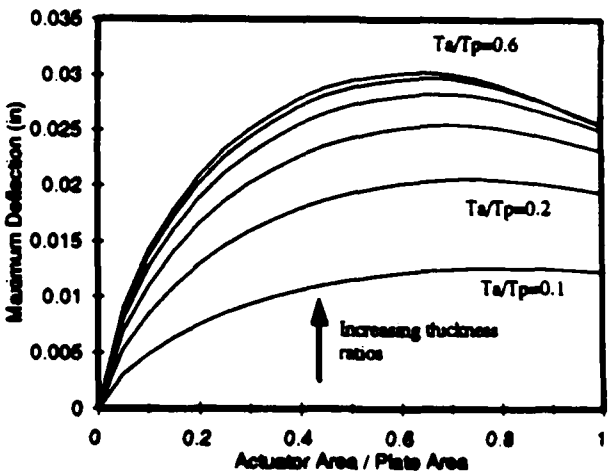

Figure 4 - Maximum panel center bending deflection vs. actuator coverage for thickness ratios between 0.1 and 0.6, in increments of 0.1; aspect ratio 1.5

The curves in Figure 4 show that a slightly smaller area ratio than 0.6 will produce nearly as much panel center deflection. Using a smaller actuator would produce a weight savings with little degradation in performance. An actuator/plate thickness ratio of 0.5 also produces its greatest deflection at 65% area coverage. Note that the deflection produced with an actuator 0.5 as thick as the plate is not much different

than that produced by an actuator whose thickness ratio is 0.6.

When the actuator has a thickness ratio of 0.1, a maximum in the curve of deflection vs. actuator coverage occurs at about 80% coverage. However, the deflection does not change much between 50-100% coverage. As the actuator thickness increases, the maximum value in the panel center deflection curve becomes more pronounced and shifts toward a smaller actuator area coverage

Figure 5 shows the results of analyses for actuator/plate thickness ratios between 0.6 and 1 for the entire area ratios between 0.1 and 1. The thickness ratio of 0.6 still produces the most deflection at area ratios greater than 50%. However, thickness ratios of 0.7 and 0.8 produce larger deflections at low actuator area coverage.

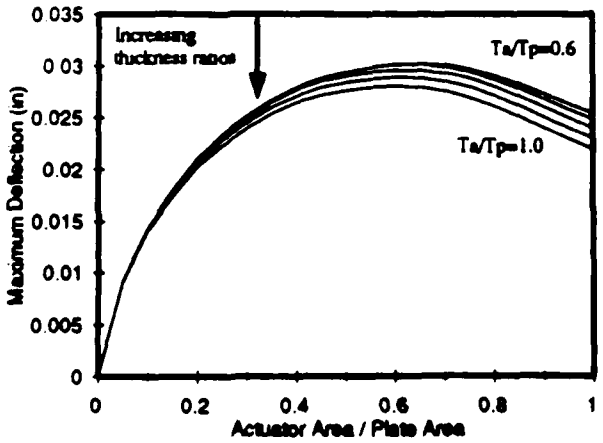

Figure 5 - Plate center bending deflection vs. actuator area coverage for thickness ratios between 0.6 and 1.0 (increments of 0.1); aspect ratio 1.5.

Effects of panel aspect ratio on optimal actuator size

Figure 6 shows the maximum panel center bending deflection obtained at an actuator/host plate thickness ratio of 0.6 for several different panel aspect ratios. Although the aspect ratio can be changed, the total plate area and actuator area remain fixed to be the same as a panel with dimensions 18 in.x 18 in. The square panel with an aspect ratio of 1 has the largest center deflection. The panel with an aspect ratio of 1.5 has a deflection smaller than that of the square panel, but the maximum bending deflection still occurs when the actuator coverage is about 65% of the plate.

The panel with a planform aspect ratio of 3 has a maximum center deflection less than half of the square panel, even though the panel areas are the same. In this case the simple supports are so close to the panel center when the aspect ratio is 3 that the stiffness of the panel is increased with respect to center deflection.

For all of the previous studies, the actuator area and aspect ratio were restrained to be the same as the plate to which it was mounted, although the actuator aspect ratio does not need to be the same. The effect of changing the actuator aspect ratio on the panel center bending deflection was examined using our model.

For the square panel, the best actuator has an actuator thickness ratio of 0.6 and an area coverage of 65%. Any actuator aspect ratio less than or greater than 1 creates a smaller center deflection than the initial configuration, although the differences are small.

When the panel aspect ratio is 1.5, the best actuator also has a thickness ratio of 0.6 and covers an area of 65% of the panel. When the actuator aspect ratio is increased so the actuator spans the long dimension of the panel, the greatest decrease in deflection is about 5.7%.

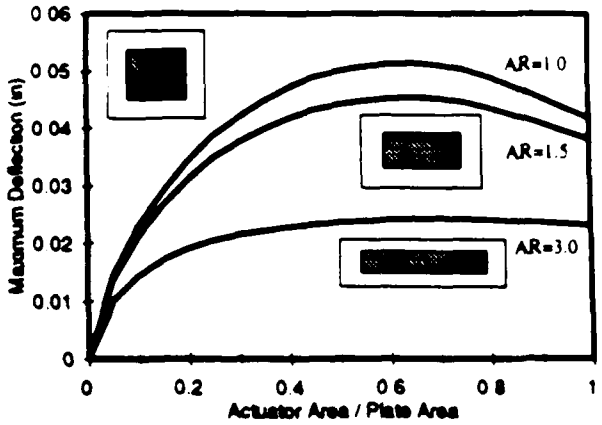

Figure 6 - The effect of actuator coverage on center deflection of three different panels; constant actuator and panel area with actuator/plate thickness ratio 0.6; aspect ratios 1, 1.5 and 3.

For a panel with an aspect ratio of 3, the best actuator has a thickness ratio of 0.6 and an area coverage of 70%. For this case, an actuator with an aspect ratio smaller than the panel produces the greatest deflection, although the increase is only 0.5%.

Non-centrally located actuators

For all previous results, the actuator was centered on the panel planform and the maximum deflection occurred in the center of the panel. For a non-centered actuator, the maximum deflection will not occur in the center of the panel, so a deflection distribution must be examined. This centerline is located in the x-direction, parallel to the long edge of the plate.

The baseline panel with an aspect ratio of 1.5 was used for a study of the effects of non centrally located actuators. The actuator has the same aspect ratio as the panel itself. Two different actuator sizes were used; they covered 6.25% and 25% of the plate area. The actuator was subjected to its maximum electric field throughout and located at one of four different locations along the centerline. In each case, the deflection profile was calculated and compared.

The smallest (6.25% area coverage) actuator was placed in the center of the panel, then shifted toward the left edge of the panel. Figure 7 shows the deflection

profile at the centerline of the panel in each case (see inset for positions). The actuator edge can be moved close to the edge of the panel without seeing a large decrease in the maximum deflection. However, once an actuator edge is at or near the panel edge, the peak deflection decreases noticeably. Since the shape and amplitude of the bending deflection on the panel can be changed by relocating the actuator this provides a way to tailor the aerodynamic shape.

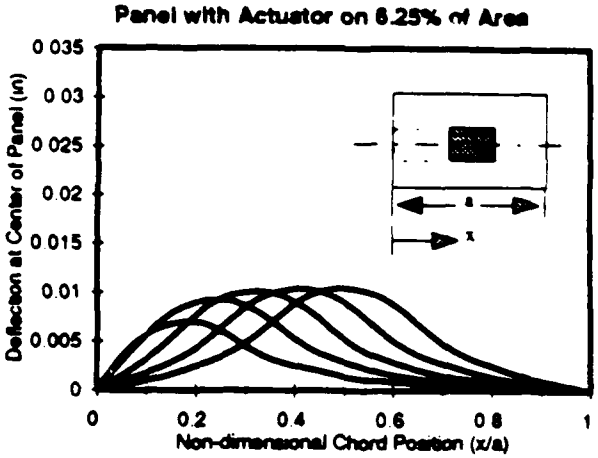

Figure 7 - Bending deflection distribution for a panel with an actuator covering 6.25% of panel.

Figure 8 shows the centerline deflection profile for the actuator covering 25% of the panel area and how this deflection changes as the actuator is repositioned along the panel centerline. The maximum deflection here is about twice that of the smaller 6.25% coverage actuator. The peak deflection when the actuator edge is at the edge of the panel is about 16% less than when the actuator is centered.

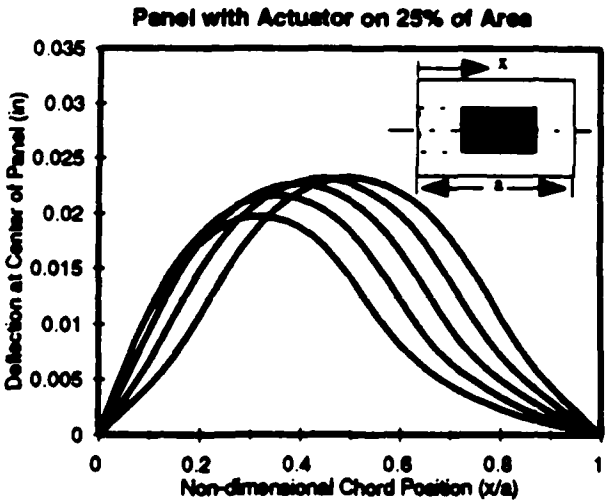

Figure 8 - Bending deflection distributions for a panel with an actuator covering 25% of panel area.

Strain energy density for optimal actuator size

We have observed that actuator thickness and panel area coverage affect the size of the panel bending deflection. When we try to create bending deflection with this type of actuator, two effects are in conflict with each other. First of all, as actuator thickness (or area) increases the actuator is able to create large strains to induce inplane forces and bending moments. On the other hand, as the actuator becomes thicker and covers more area, the panel stiffness also increases so that the plate is more difficult to bend.

When the actuator is small compared to the plate, its attempt to expand is easily thwarted by a relatively massive plate. When a voltage is applied to the actuator, most of the strain energy comes from the actuator being held relatively fixed and expanding only inplane where the inplane stiffness is larger than the actuator bending stiffness. Very little strain energy goes into bending.

On the other hand, as the actuator grows in size, the rate of change of induced bending moment with respect to actuator thickness is relatively large compared to the rate of change of panel bending stiffness. As a result, it is better to increase the size of the actuator and more energy goes into bending. Bending stiffness is much less than inplane stiffness so the rate of change of strain energy with respect to changes in actuator thickness becomes less.

As the actuator thickness increases, the bending stiffness increases more rapidly than the induced moment. At some point, the rate of change of induced bending moment will equal the rate of change in bending stiffness. This is the best actuator for bending deflection. Any increase in actuator size will increase bending stiffness more than induced bending moment and will be counter-productive. The actuator becomes non-optimal.

The dependence of panel strain energy on actuator thickness can be plotted for a panel with two parallel edges free while the other two edges are simply supported. This is the case called cylindrical bending. When the actuator covers the entire plate area, the resulting deflection when the actuator is operated at its full power is a parabola with constant curvature. The expression for strain energy of this special plate is as follows:

$$U = \frac{1}{2}\iint\left[A_{11}\left(\frac{\partial u_o}{\partial x}\right)^2 - 2B_{11}\frac{\partial u_o}{\partial x}\frac{\partial^2 w}{\partial x^2} + D_{11}\left(\frac{\partial^2 w}{\partial x^2}\right)^2 - 2N_{xA}\frac{\partial u_o}{\partial x} + 2M_{xA}\frac{\partial^2 w}{\partial x^2} + \sum_{k=1}^{N} E^{(k)}\left(\Lambda_1^{(k)}\right)^2 t_k\right]dxdy \tag{10}$$

Consider the case of a constant thickness aluminum plate with a PZT actuator covering one 100% of the plate. The strain energy (U divided by the area of the plate) is plotted in Figure 9 against actuator thickness ratio. Also plotted is the curvature of the plate vs. thickness ratio.

The maximum bending deflection occurs when the plate curvature is a maximum and when the actuator

thickness ratio is 0.5. The strain energy density has an inflection point at this thickness ratio.

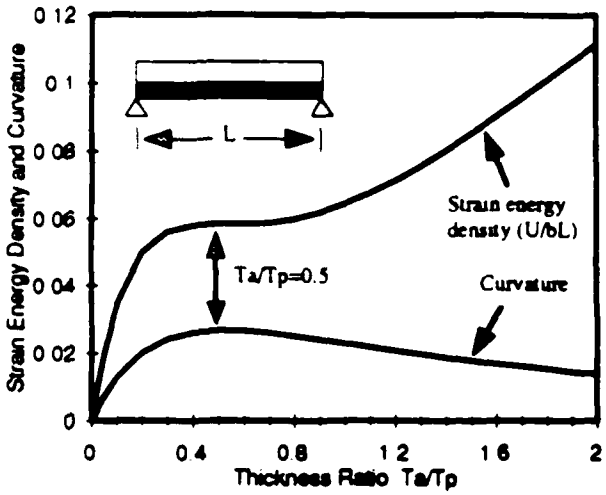

Figure 9 - Beam strain energy density and curvature vs. actuator/plate thickness ratio. Full coverage actuator; cylindrical bending.

The presence of an inflection point is important because it suggests an optimality criterion to select the actuator. The "too small" actuator stores a large part of the mechanical energy because the panel barely deforms. When the actuator reaches a "critical size" the panel bends a great deal, but stores energy in a more "flexible" mode. As actuator size increases further, the dominant energy storage mode again becomes extensional and the slope of the strain energy density curve turns upward and increases rapidly.

The favorable bending energy storage mode is identified by an inflection point or "flat spot" in the strain energy density vs. actuator thickness curve.

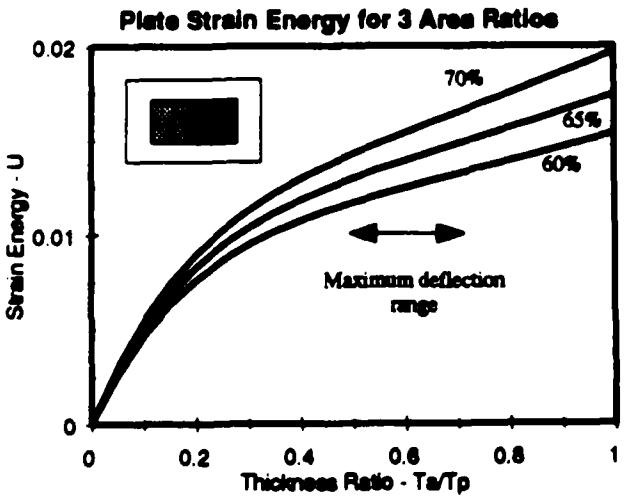

Figure 10 - Plate strain energy vs. actuator thickness ratio for 60%, 65% and 70% area coverage. Panel aspect ratio is 1.5.

The strain energy for the plate can also be plotted versus thickness ratio. Figure 10 shows the strain energy plotted vs. thickness ratio for actuators covering 60%, 65%, and 70% of the plate area for an aluminum plate with an aspect ratio of 1.5. In the cylindrical bending case, it was possible to identify the best thickness ratio by looking for an inflection point in the strain energy plot. However, this inflection point is not so evident for the simply supported panel.

The curves in Figure 10 become nearly linear for larger thickness ratios. Figure 10 indicates that, as long as the slope of the strain energy curve is changing with increases in thickness ratios, adding thickness to the actuator will be beneficial. But once the curve becomes linear, adding actuator thickness will not produce more bending deflection in the panel.

Conclusions

A panel with a self-straining actuator mounted on one side was studied to find the features of the actuator that produces the largest deflection of simply supported rectangular panels. A Rayleigh-Ritz model was developed to compute inplane and bending deflections of a plate with an actuator covering only part of the area.

It was shown that it is important to include the coupling terms and the in-plane actuator forces to accurately model the problem. A simple polynomial assumed displacement field provided good agreement with the finite element results for centrally located actuators with a large area coverage.

To match the finite element results for smaller actuator areas and to provide more accurate results overall, a Rayleigh-Ritz trigonometric series expansion was developed. This model allows the actuator to be placed at any location on the panel. It was found that a series with $M = N = 11$ terms for each of the u, v, and w displacements yielded excellent results, very close to those of the NASTRAN program.

For aluminum panels with aspect ratios between 1.0 and 1.5, the best actuator has a thickness ratio of 0.6 and covers 65% of the panel area. For a panel with an aspect ratio of 3.0, the best actuator has a thickness ratio of 0.6 and covers 70% of the area. For the panels with aspect ratios of 1.0 and 1.5, the actuator with the same aspect ratio as the panel produced the largest deflection. For the panel of aspect ratio 3.0, an actuator with an aspect ratio slightly smaller than that of the panel produced the most deflection.

The effect of actuator location on the deflection profile of a simply supported panel was examined. An actuator with 25% area coverage or less produced the most change in the bending deflection shape.

For a plate with cylindrical bending, when the strain energy is plotted against thickness ratio, the curve shows an inflection point at the best actuator thickness for that configuration. Although the best actuator thickness was obviously at the inflection point in the strain energy curve for the cylindrical bending case, the best actuator thickness for the general plate was less

best actuator thickness for the general plate was less obvious.

The plot of strain energy vs. actuator thickness ratio becomes nearly linear at the point corresponding to the best actuator thickness ratio. This indicated that increasing the thickness of the actuator was beneficial until the slope of the strain energy curve reached its smallest value. Adding more thickness to the actuator beyond this point increases stiffness more than it increased the applied moments, and does not increase the deflection that is obtained in the panel.

For this study, actuator thickness, area, and aspect ratio were varied to find which combination produced the largest deflection in a given panel. More precise results for the actuator characteristics could be calculated if an optimization scheme were used in conjunction with the model already developed. Since only a finite number of combinations were tried in this study, the best actuator was found within the limits of the study. Also, the optimal actuator could be found by taking into consideration the weight that is added for a larger actuator. A larger, thicker actuator does not always produce significantly more deflection than a smaller, lighter actuator.

This study was also limited to rectangular actuators placed at any location on the panel. Actuators of shapes other than rectangular should also be considered. Rectangular actuators produce high stresses at the edges and corners[17]. The corner stresses might be avoided if the actuator shape were changed. The deflection produced by elliptical actuators or other actuator shapes should be examined.

The plate deflections obtained here used the PZT actuators to their fullest extent, applying voltages to the actuators that are right at their capabilities. Much needs to be done to improve the efficiency of these materials. On the other hand, we do believe that there is promise for future applications to high speed flow control.

Acknowledgment

This research was supported, in part, by the Air Force Office of Scientific Research under AFOSR Grant 91-0386. Dr. Spencer Wu was contract monitor.

References

1. Muller, M. and Weisshaar, T.A., "Transonic Drag Reduction Through the Use of Induced Strain Actuators to Form an Adaptive Airfoil," AIAA Paper 94-1775, AIAA/ASME Adaptive Structures Forum, Hilton Head, South Carolina, April 1994.

2. Sobieczky, H. and Dulikravich, G.S., "Transonic Airfoil Thickness Variation Requirements for Maintaining Shock-free Flow," in Smart Materials and Structures 1993: Smart Structures and Intelligent Systems, Nesbitt W. Hagood and Gareth J. Knowles, Editors, Proc. SPIE 1917, Vol. 1, pp. 119- 124, 1993.

3. Scott, R.C., "Control of Flutter Using Adaptive Materials," M.S. Thesis, Purdue University, West Lafayette, Indiana, May 1990.

4.. Abou-Amer, S.A., "Control of Panel Flutter at High Supersonic Speed," Ph.D. Dissertation, Illinois Institute of Technology, Chicago, Ill., Dec. 1991.

5. Paige, D., "Active Control of Composite Panel Flutter Using Piezoelectric Materials," M.S. Thesis, Purdue University, West Lafayette, Indiana, May 1992.

6. Hajela, P. and Glowasky, R., "Application of Piezoelectric Elements in Supersonic Panel Flutter Suppression," AIAA Paper No. 91-3191, AIAA/AHS/ASEE Aircraft Design Systems and Operations Meeting, Baltimore, Md., Sept., 1991.

7. Scott, R. C. and Weisshaar, T. A., "Controlling Panel Flutter Using Adaptive Materials," Proceedings of the 32nd Structures, Structural Dynamics and Materials Conference, Baltimore, Md., April 1991.

8. Kim, S. J., and Jones, J. D., "Optimal Design of Piezoactuators for Active Noise and Vibration Control," *AIAA Journal*, Vol. 29, No. 12, December, 1991, pp. 2047-2053.

9. Rogers, C. A., Liang, C., and Jia, J., "Behavior of Shape Memory Alloy Reinforced Composite Plates Part I: Model Formulations and Control Concepts," AIAA Paper No. 89-1389-CP.

10. Crawley, E. F., and Lazarus, K. B., "Induced Strain Actuation of Isotropic and Anisotropic Plates," AIAA Paper No. 89-1326-CP, 1989.

11. Wang, B. T., and Rogers, C. A., "Laminate Plate Theory for Spatially Distributed Induced Strain Actuators," *Journal of Composite Materials*, Vol. 25, April 1991, pp. 433-452.

12. Vasiliev, V. V., *Mechanics of Composite Structures*, Taylor and Francis, Washington, D.C., 1993

13. Sun, C. T., and Chin, H., On Large Deflection Effects in Unsymmetric Cross-Ply Composite Laminates, *Journal of Composite Materials*, Vol. 22, November, 1988, pp. 1045-1059.

14. Sun, C. T., and Chin, H., Analysis of Asymmetric Composite Laminates, *AIAA Journal*, Vol. 26, NO. 6, June 1988, pp. 714-718.

15. Hetnarski, R.B., Editor, *Thermal Stresses I*, Elsevier Science Publishers, B.V., 1986.

16. Whitney, J. M., *Structural Analysis of Laminated Anisotropic Plates*, Technomic Publishing Co., Inc., 1987.

17. Leeks, T.J., "Optimal Design of Partial-Plate Piezoelectric Actuators for Maximum Panel Deflection," M.S. Thesis, Purdue University, Dec. 1993.

Appendix - Strain Energy Expression

Nomenclature

a	plate length
A_{ij}	extensional stiffness matrix
A, A_{mn}	assumed series solution constants
b	plate width
B_{ij}	coupling stiffness matrix
B, B_{mn}	assumed series solution constants
C, C_{mn}	assumed series solution constants
d_{31}	piezoelectric constant
D_{ij}	bending stiffness matrix
E_3	electric field strength
N_{xA}, N_{yA}, N_{xyA}	piezoelectric inplane forces
M_{xA}, M_{yA}, M_{xyA}	piezoelectric moments
$\overline{Q}_{ij}^{(k)}$	reduced lamina stiffness for kth layer
T_a	actuator thickness
T_p	host plate thickness
u_o	inplane deflection in x direction
U	panel strain energy
v_o	inplane deflection in y direction
w	bending deflection
$\Lambda_i^{(k)}$	piezoelectric strain of kth lamina

The strain energy expression, U, is used to compute the mechanical strain for a plate/actuator combination in plane stress when the piezoelectric actuator creates induced strain. The mechanical strain is the difference between the total strain and the expansion strain, and is the only strain that creates stress[16]. There is no stress induced if the material is allowed to expand freely. The induced piezoelectric strains are analogous to thermal strains.

To compute strain energy, a reference surface at the mid-plane of the host plate was chosen. This allows the reference surface to remain fixed when the actuator thickness changes thus reducing computational complexity. The last three terms of the equation are independent of the displacements u, v, and w. The integral involving these terms will vanish under the first variation of the strain energy and the terms will not enter the equations when the Rayleigh-Ritz method is applied. For this analysis a rectangular actuator is attached to a plate at an arbitrary position.

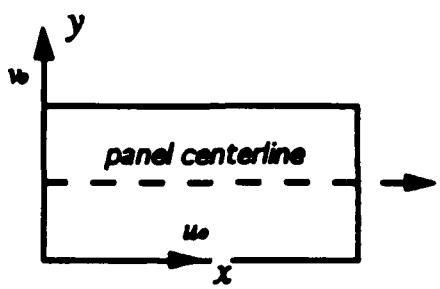

$$U = \frac{1}{2}\iint [A_{11}\left(\frac{\partial u_o}{\partial x}\right)^2 + 2A_{12}\frac{\partial u_o}{\partial x}\frac{\partial v_o}{\partial y} + A_{22}\left(\frac{\partial v_o}{\partial y}\right)^2 + 2A_{16}\frac{\partial u_o}{\partial x}\left(\frac{\partial u_o}{\partial y} + \frac{\partial v_o}{\partial x}\right)$$

$$+2A_{26}\frac{\partial v_o}{\partial y}\left(\frac{\partial u_o}{\partial y} + \frac{\partial v_o}{\partial x}\right) + A_{66}\left(\frac{\partial u_o}{\partial y} + \frac{\partial v_o}{\partial x}\right)^2 - 2N_{xA}\frac{\partial u_o}{\partial x} - 2N_{yA}\frac{\partial v_o}{\partial y} \quad \text{(continued)}$$

$$-2N_{xy\Lambda}\left(\frac{\partial u_o}{\partial y}+\frac{\partial v_o}{\partial x}\right)-2B_{11}\frac{\partial u_o}{\partial x}\frac{\partial^2 w}{\partial x^2}-2B_{12}\left(\frac{\partial v_o}{\partial y}\frac{\partial^2 w}{\partial x^2}+\frac{\partial u_o}{\partial x}\frac{\partial^2 w}{\partial y^2}\right)$$

$$-2B_{22}\frac{\partial v_o}{\partial y}\frac{\partial^2 w}{\partial y^2}-2B_{16}\left(\left(\frac{\partial u_o}{\partial y}+\frac{\partial v_o}{\partial x}\right)\frac{\partial^2 w}{\partial x^2}+2\frac{\partial u_o}{\partial x}\frac{\partial^2 w}{\partial x\partial y}\right)$$

$$-2B_{26}\left(\left(\frac{\partial u_o}{\partial y}+\frac{\partial v_o}{\partial x}\right)\frac{\partial^2 w}{\partial y^2}+2\frac{\partial v_o}{\partial y}\frac{\partial^2 w}{\partial x\partial y}\right)-4B_{66}\frac{\partial^2 w}{\partial x\partial y}\left(\frac{\partial u_o}{\partial y}+\frac{\partial v_o}{\partial x}\right)$$

$$+D_{11}\left(\frac{\partial^2 w}{\partial x^2}\right)^2+2D_{12}\frac{\partial^2 w}{\partial x^2}\frac{\partial^2 w}{\partial y^2}+D_{22}\left(\frac{\partial^2 w}{\partial y^2}\right)^2+4D_{16}\frac{\partial^2 w}{\partial x^2}\frac{\partial^2 w}{\partial x\partial y}$$

$$+4D_{26}\frac{\partial^2 w}{\partial y^2}\frac{\partial^2 w}{\partial x\partial y}+4D_{66}\left(\frac{\partial^2 w}{\partial x\partial y}\right)^2+2M_{x\Lambda}\frac{\partial^2 w}{\partial x^2}+2M_{y\Lambda}\frac{\partial^2 w}{\partial y^2}$$

$$+4M_{xy\Lambda}\frac{\partial^2 w}{\partial x\partial y}+\sum_{k=1}^{N}\overline{Q}_{11}^{(k)}\left(\Lambda_1^{(k)}\right)^2\left(z_k-z_{k-1}\right)$$

$$+2\sum_{k=1}^{N}\overline{Q}_{12}^{(k)}\Lambda_1^{(k)}\Lambda_2^{(k)}\left(z_k-z_{k-1}\right)+\sum_{k=1}^{N}\overline{Q}_{22}^{(k)}\left(\Lambda_2^{(k)}\right)^2\left(z_k-z_{k-1}\right)\Big]dxdy \quad \text{(concluded)}$$